Energy Reviews 4 (2025) 100129

Contents lists available at ScienceDirect

Energy Reviews

journal homepage: www.journals.elsevier.com/energy-reviews

Full Review Article

Status and prospects of anode materials for efficient electrochemical ozone production

Xiuyue Wang [a,1], Ye Yuan [b,1], Zheyuan Ding [c], Junna Yang [a], Yilin Wang [a], Siming Li [d], Yu Ding [d], Yawei Li [d,*], Min Wang [a,**], Mingbo Wu [a,***]

[a] College of New Energy, China University of Petroleum (East China), Qingdao, 266580, China
[b] Jinan Ourui Industry Co., Ltd., Jinan, 250100, China
[c] Key Laboratory for Green Chemical Technology of Ministry of Education, School of Chemical Engineering & Technology, Collaborative Innovation Center for Chemical Science & Engineering, Tianjin University, Tianjin, 300072, China
[d] School of Chemistry and Chemical Engineering, Shanxi University, Taiyuan, 030001, China

ARTICLE INFO

Keywords:
Electrochemical ozone production
Lead-based catalysts
Platinum and its alloys
Doped tin dioxide
Boron-doped diamond

ABSTRACT

Utilizing efficient and eco-friendly electrochemical techniques for the synthesis of valuable chemicals represents an optimal strategy for enhancing energy utilization. Electrochemical ozone production (EOP), recognized for its cleanliness and adaptability, emerges as a promising energy conversion technology for the synthesis of high-value chemicals. However, the selection of anode materials poses a significant challenge to the widespread commercial deployment of EOP, and a thorough investigation into this area is crucial for improving both the performance and durability. In this review, we delve into the fundamental principle of ozone generation, explore the advantages and constraints associated with various EOP systems, and discuss how the utilization of advanced membrane electrode assembly (MEA) electrolysis cells can sustain an overall efficiency of 20 % or higher. This review offers objective evaluations of various anode materials and summarizes recent advancements in EOP, highlighting laboratory-measured current efficiencies that surpass 50 %. Lastly, this review delineates the myriad challenges encountered within the current EOP research and proposes potential avenues for future development, all in an effort to furnish indispensable insights for the industrial implementation of EOP.

1. Introduction

Ozone is a high value-added chemical with a redox potential of up to 2.07 V, making it one of the strongest oxidants, surpassed only by fluorine and hydroxyl radicals [1–3]. This potent oxidative capability endows ozone with a significant role in practical applications. Ozone possesses the advantages of being environmentally friendly, producing only oxygen as a by-product, which is harmless to the environment. The use of this clean disinfectant aligns with the global trend toward carbon neutrality [4]. The integration of renewable energy generation technologies with the process of ozone production could further boost ozone's appeal for environmental applications. The literatures have demonstrated the effective amalgamation of boron-doped diamond (BDD) electrochemical flow cells with photovoltaic power generation systems, underscoring the practical feasibility and theoretical potential of coupling electrochemical ozone production (EOP) with renewable energy technologies [5–7]. Leveraging these advantages, ozone has been widely employed across multiple applications and industries. In sterilization and disinfection, ozone effectively eradicates bacteria, viruses, and other microorganisms [8–10]. Its strong oxidative properties efficiently remove organic and inorganic pollutants without causing adverse side effects [11–13] in the water treatment process. In air pollution control, ozone demonstrates strong efficacy in treating pyridine exhaust gases [14] and nitrogen oxides in biodiesel [15]. Furthermore, ozone is applied in the food processing industry for sterilization and preservation, extending the shelf life of food products [16–18]. The exceedingly strong oxidative nature of ozone resulted in significant instability of its chemical properties, facilitating rapid decomposition into oxygen under standard conditions. In aqueous solution, ozone has a half-life of approximately 16 min [19–21].

* Corresponding author.
** Corresponding author.
*** Corresponding author.
E-mail addresses: yaweili@sxu.edu.cn (Y. Li), minwang@upc.edu.cn (M. Wang), wumb@upc.edu.cn (M. Wu).
[1] These authors contributed equally.

https://doi.org/10.1016/j.enrev.2024.100129
Received 15 October 2024; Received in revised form 2 December 2024; Accepted 30 December 2024

Abbreviation

BDD	Boron-doped diamond
EOP	Electrochemical ozone production
DBD	Dielectric barrier discharge
UV	Ultraviolet
SPE	Solid polymer electrolyte
DFT	Density functional theory
MEA	Membrane electrode assembly
OER	Oxygen evolution reaction
PEM	Proton exchange membrane
AAO	Anodic aluminum oxide
CFD	Computational fluid dynamics
BPP	Bulk porous Pb
CVD	Chemical vapor deposition
HPHT	High-pressure high-temperature
p-BDD	Porous boron-doped diamond

This instability necessitates its on-site production in most cases [22].

Dielectric barrier discharge (DBD) is a commonly utilized method in industrial ozone production, mimicking the natural process of ozone generation through lightning-induced air breakdown [23,24]. Its principle revolves around the utilization of an alternating high-voltage electric field to induce corona discharge in oxygen-containing gas. During the corona discharge, high-energy free electrons dissociate oxygen molecules, thereby facilitating the formation of ozone molecules [25,26]. The reaction process can be briefly summarized as follows:

$$O_2 + e^-(\text{High} - \text{energy electron}) \rightarrow 2O + e^-(\text{Low} - \text{energy electron}) \quad (1.1)$$

$$O + O_2 + M \rightarrow O_3 + M \quad (1.2)$$

where M represents an intermediate product involved in the reaction.

DBD methods for ozone generation have the advantages of high generation capacity and are suitable for large-scale industrialization [27,28]. While achieving industrial production within a certain range, the DBD method inevitably processes some drawbacks. Ozone production via DBD necessitates reactions under high-pressure and high-energy conditions [29,30], demanding significant energy input and resulting in high energy consumption. Additionally, ozone's rapid decomposition under high-temperature conditions necessitates the inclusion of efficient cooling systems in the equipment. The inclusion of the required sub-system within the main processing systems enlarges the equipment, complicates its mobility, and generates noise. Furthermore, the raw gas requires preprocessing procedures, including compression and drying [31], rendering the preparation process complex. While ozone production via this method is substantial, the concentration remains low, thus unable to fulfill the demand for high-concentration ozone. When air is used as the raw gas, toxic nitrogen oxides are also produced, posing irreversible harm to human health [32,33].

Ultraviolet (UV) irradiation simulates the atmospheric ozone generation process through sunlight-induced UV radiation. The principle involves irradiating dried oxygen molecules with UV light of specific wavelengths, resulting in the partial decomposition of oxygen molecules into oxygen atoms. Subsequently, these oxygen atoms combine with the remaining oxygen molecules to form ozone [34]. The reaction process can be summarized as follows:

$$O_2 + h\nu \rightarrow 2O \quad (1.3)$$

$$O + O_2 + M \rightarrow O_3 + M \quad (1.4)$$

where M represents an intermediate product involved in the reaction.

$$O + O_3 \rightarrow 2O_2 \quad (1.5)$$

Utilizing UV irradiation for ozone generation requires operation within a specific wavelength range. This method allows for the regulation of ozone concentration and generation capacity by adjusting the output power of UV lamps, providing the advantages of easy control and stable output. Additionally, this method exhibits good reproducibility and insensitivity to environmental factors such as temperature and humidity [35]. However, a notable drawback of UV irradiation is its high energy consumption, resulting in relatively low ozone generation capacity and concentration, and rendering it unsuitable for large-scale production. Furthermore, this method is only suitable for small-scale applications due to the limited power and short lifespans of UV lamps.

Utilizing efficient and environmentally friendly electrochemical strategies to produce high-value chemicals is an ideal approach for maximizing resource utilization [36,37]. Electrochemical synthesis of urea presents an emerging alternative technology to traditional processes in the fossil energy industry for urea production, effectively reducing carbon emissions [38,39]. Similarly, EOP shows promise as an environmentally friendly method [40–42]. By adjusting reaction conditions and catalyst types, it is possible to produce ozone of higher value compared to oxygen. In the early stages of EOP development, challenges such as the intricacies of electrolyte formulation and the limitations of ozone generation capacity significantly impeded its widespread application. However, the swift progression in the field of solid polymer electrolyte (SPE) technology [43–46] has enabled EOP to surmount these technological barriers, thereby positioning itself as a formidable contender in the realm of ozone generation. Despite these remarkable advancements, the challenges related to the economic viability and the production yield remain significant obstacles to the large-scale industrialization of EOP technology. The exorbitant expense associated with SPE materials, coupled with the suboptimal efficiency of ozone generation processes, persist as critical limiting factors impeding the extensive deployment of EOP technology. To address these issues, ongoing research endeavors are diligently focused on the refinement of SPE design, the exploration of more cost-effective materials, and the improvement of the efficacy of ozone production methodologies. Future developments in the field are anticipated to encompass the implementation of materials. These materials are more fiscally prudent, as well as the adoption of innovative manufacturing techniques aimed at diminishing production costs. Moreover, the anticipated advancements in the realms of system integration and automation are poised to significantly enhance the scalability of EOP systems, thereby increasing production yield and bolstering their commercial viability.

EOP involves a typical six-electron reaction [47,48], with the anodic reaction equations as follows:

$$2H_2O \rightarrow O_2 + 4H^+ + 4e^- \quad E^0 = +1.23\ \text{V} \quad (1.6)$$

$$3H_2O \rightarrow O_3 + 6H^+ + 6e^- \quad E^0 = +1.51\ \text{V} \quad (1.7)$$

The cathodic reaction equation is as follows:

$$2H^+ + 2e^- \rightarrow H_2 \quad E^0 = 0\ \text{V} \quad (1.8)$$

EOP offers several advantages over other conventional methods. These advantages include equipment simplicity, low investment costs, mobility, and adaptability to a wider range of applications [49]. EOP provides convenience in preparation and on-site production, along with generating ozone of higher purity [50,51], where oxygen is the sole by-product. This characteristic avoids the formation of toxic substances, promoting environmental friendliness and offering vast potential for various applications [22,52,53]. The differences between DBD, UV irradiation and EOP in terms of production capacity, scalability, by-products and cost are summarized in Table 1.

Various factors influence EOP performance, with M. Rodríguez-Pena et al. [54] specifically investigating the impact of electrolyte on EOP

Table 1
Comparison of different ozone production methodologies.

Relevant parameters	DBD	UV	EOP
Production capacity	Suitable for industrial-scale applications with high production capacity	Limited actual production capacity	Production capacity can be increased in large-scale applications, but is constrained by anode material selection
Scalability	Good scalability for industrial applications	Limited prospects for large-scale production	Highly scalable with advanced electrode technology
By-products	Hazardous nitrogen oxides	Nitrogen oxides	Oxygen
Cost	Costly initial setup	Lower cost	Higher cost of anode materials and MEA

performance. Their findings suggest that the highest ozone generation capacity is achieved by using a 1.0 M perchloric acid solution, attributed to the absence of ozone scavengers in perchloric acid, which effectively enhances the stability of dissolved ozone. In a separate study, M. Rodríguez-Pena et al. [55] conducted an in-depth investigation into the influence of pressure. Ozone production demonstrates an increasing trend with rising pressure, mainly due to the faster increase in the ozone dissolution rate compared to that of oxygen as pressure rises. However, current EOP systems exhibit poor stability and significant energy consumption, falling short of industrial production requirements. Additionally, much attention is directed towards the impact of various anode materials on EOP performance. Due to the extensive potential of EOP applications, we classified different types of anode materials based on their substrate according to existing literature. We briefly explained the operational philosophy of EOP, summarized recent advancements in EOP anode materials, and outlined future prospects. Expected to offer valuable insights for the industrial implementation of EOP.

2. Overview of electrochemical ozone production

2.1. Reaction mechanism

In the electrochemical production of ozone, the electrolyte undergoes oxidation under the influence of applied electric current, resulting in the generation of ozone and oxygen at the anode, as depicted in equations (1.6) and (1.7). The mechanism of the EOP reaction proposed by L. M. Da Silva et al. [56] is widely accepted among researchers. However, this mechanism remains speculative due to the incomplete consideration of practical influences in many reaction processes, such as the effect of bubble residence time during the reaction and the mechanism by which electrode materials facilitate the formation of ozone through interaction with oxygen intermediates, as summarized in Table 2. Recently, Zhang et al. [57] have conducted further research on the mechanism of EOP, expanding on prior studies. They discovered that the mechanism can be illustrated by an electrocatalytic five-membered ring, as depicted in Fig. 1a. The production of ozone overall can be segmented into four reaction steps:

Table 2
Mechanism of EOP/OER reactions.

Reaction steps	Reaction formula
Kinetically controlled steps	$H_2O \rightarrow (OH\cdot)_{ads} + H^+ + e^-$ $(OH\cdot)_{ads} \rightarrow (O\cdot)_{ads} + H^+ + e^-$
Efficiency controlled steps	$(O\cdot)_{ads} \rightarrow [1-\theta]\ (O\cdot)_{ads} + \theta(O\cdot)^*_{ads}\ (0<\theta<1)$ $[1-\theta]\ (2O\cdot)_{ads} \rightarrow [1-\theta]\ (O_2)_{ads}$ $[1-\theta]\ (O_2)_{ads} \rightarrow [1-\beta]\ [1-\theta]\ (O_2)_{ads} + \beta[1-\theta]\ (O_2)^*_{ads}$ $(0<\beta<1)$
OER	$[1-\beta]\ [1-\theta]\ (O_2)_{ads} \rightarrow O_2\uparrow$
EOP	$\theta(O\cdot)^*_{ads} + \beta[1-\theta]\ (O_2)^*_{ads} \rightarrow [\theta+\beta[1-\theta]]\ (O_3)_{ads}$ $[\theta+\beta[1-\theta]]\ (O_3)_{ads} \rightarrow O_3\uparrow$

$$H_2O \rightarrow OH^* + H^+ + e^- \quad (1.9)$$

$$OH^* \rightarrow O^* + H^+ + e^- \quad (1.10)$$

$$2O^* \rightarrow {O_2}^* \rightarrow O_2 \quad (1.11)$$

$${O_2}^* + O^* \rightarrow {O_3}^* \rightarrow O_3 \quad (1.12)$$

The initial stage of the reaction primarily involves the decomposition of H_2O^* and OH* and the formation of O* intermediates. By conducting density functional theory (DFT) calculations on the reaction energy barriers for each step, as depicted in Fig. 1b, OH* can undergo deprotonation to produce O* and H*, with a reaction energy barrier of 0.3 eV. Given the relatively low reaction energy barrier, this step can occur almost spontaneously. In contrast, the energy barriers for the formation of oxygen and ozone are relatively high, rendering the formation process more challenging. This is a contributing factor to the limited increase in ozone production thus far.

Building on an understanding of the prevailing mechanisms of EOP, an exemplary catalyst for this process must embody a multitude of crucial attributes. Firstly, the catalyst must promote the adsorption of water molecules on its surface and facilitate their effective deprotonation, thereby providing the necessary protons for the subsequent oxidation reaction. Secondly, the catalyst is required to exhibit a balanced chemisorption affinity for oxygen-related reactive intermediates, which is pivotal for the stabilization of oxygen molecules on the electrode surface, thereby enabling their effective aggregation into ozone. Moreover, it is imperative that the catalyst exhibits a weak chemisorption tendency towards ozone, thereby preventing excessive adsorption and ensuring subsequent decomposition on the electrode surface. Furthermore, the catalysts should also possess excellent electronic and ionic conductivity to support efficient electrochemical reactions, as well as robust corrosion resistance and long-term stability to ensure their longevity in highly oxidative environments. Lastly, the catalyst must demonstrate cost-effectiveness and scalability, two critical factors that enable its large-scale industrial deployment. It is only through the synergistic integration of these attributes that the catalyst can achieve optimal performance in EOP, thereby facilitating the extensive adoption of this innovative technology across various industrial sectors.

2.2. Ozone electrolysis cell

Improving the efficacy of the reaction apparatus stands as a pivotal research domain within the field of EOP. The quality of the reaction equipment plays a crucial role in the efficiency of ozone production, with superior apparatuses leading to enhanced production yields. Various electrochemical devices, ranging from basic single-chamber electrolysis cells to the H-type and state-of-the-art membrane electrode assembly (MEA) electrolysis cells, are utilized in EOP to improve ozone purity, reduce generation capacity, and drive the industrialization of EOP forward. The advantages and disadvantages of different types of electrolytic cells are summarized in Table 3.

The single-chamber ozone electrolysis cell is straightforward in terms of system design and thus easy to install. It was the first device created for ozone generation [58]. Fig. 1c elucidates the defining characteristic of the single-chamber ozone electrolysis cell, which is its unique structure that situates both the platinum anode and lead cathode within the same cell, in direct contact with the electrolyte solution. The single-chamber configuration minimizes the reliance on diaphragms, thereby reducing associated costs. However, the absence of a diaphragm leads to a mixed product gas of oxygen, ozone, and hydrogen, resulting in a low ozone concentration and the requirement for complex separation processes.

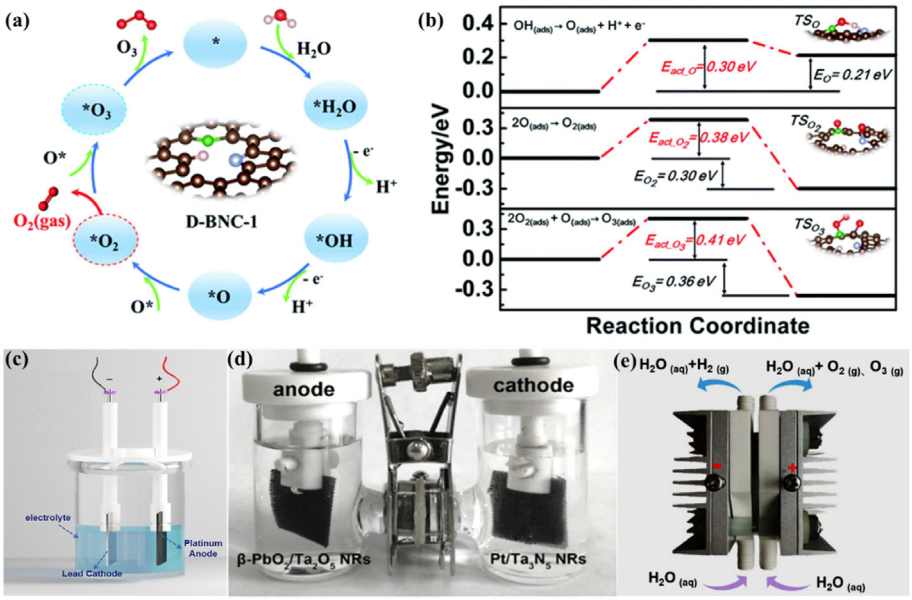

Fig. 1. (a) OER/EOP reaction mechanism (b) energy barriers in the ozone generation process, reproduced from Ref. [57] (c) schematic diagram of single-chamber ozone electrolysis cell (d) image of H-type ozone electrolysis cell, reproduced from Ref. [59] (e) schematic diagram of MEA ozone electrolysis cell, reproduced from Ref. [82].

Table 3
Advantages and disadvantages of different ozone electrolysis cells.

Ozone Electrolysis Cells	Advantages	Disadvantages
Single-chamber	Simple structure Small volume Low cost	Low product purity Gas separation difficulty Safety hazard
H-type	Effective product separation Fewer by-products	Limited production efficiency Industrial impracticality
MEA	Compact and modular design High current efficiency	High cost System complexity

Additionally, the simple construction of the single-chamber electrolysis cells tends to neglect critical hydrodynamic considerations. Static designs, as frequently discussed in academic literature, fail to account for the accumulation of gas bubbles on the electrode surface—a phenomenon that impedes mass transfer, decelerates the reaction kinetics, and reduces electrode efficiency. These inherent limitations render the suitability of the cell for practical applications, given the constraints they impose on operational efficiency and product purity.

The H-type ozone electrolysis cell, a prevalent apparatus in laboratory settings for ozone generation [57,59], as shown in Fig. 1d, consists of a cathode chamber, an anode chamber, and a diaphragm with electrolyte circulating through these components. In contrast to the single-chamber ozone electrolysis cells, the H-type ozone electrolysis cell exhibits higher EOP efficiency and a more consistent ozone generation capacity. The diaphragm plays a crucial role in reducing side reactions, preventing the diffusion and mixing of reactants and products, thereby improving the purity of the ozone produced. However, the H-type ozone electrolysis cell encounters certain limitations; the introduction of a diaphragm increases the solution resistance, which in turn leads to increased energy consumption and poses constraints on its scalability. Additionally, the H-type ozone electrolysis cells face challenges when it comes to sustained industrial application. Due to design limitations, issues such as the uneven gas distribution and a reduced reaction efficiency are likely to emerge when multiple units are connected in series or parallel, which in turn impacts their scalability and economic viability.

Fig. 1e illustrates a schematic diagram of a MEA ozone electrolysis cell. The key components mainly include bipolar plates, electrodes, catalytic layers and a proton exchange membrane (PEM), each playing a pivotal role in the cell's functionality. The MEA ozone electrolysis cell, in comparison to traditional electrochemical ozone generation devices, is featured by its compact design [44] and superior current efficiency. Owing to these distinct advantages, the MEA ozone electrolysis cell has rapidly emerged as a highly promising reaction device in the field of EOP [60,61]. The research by Wang et al. [62] summarizes the application spectrum of ozone electrolysis cells, revealing that the overall current efficiency of MEA ozone electrolysis cells hovers approximately 20 %, a figure that is about double the efficiency of H-type electrolysis cells. Nevertheless, the MEA ozone electrolysis cell encounters unresolved issues during practical operations. For instance, the presence of competition from the oxygen evolution reaction (OER) results in a decrease in ozone concentration and an inability to attain the current efficiency projected by theoretical calculations. Resolving these challenges necessitates the discovery of suitable anode materials that can ensure heightened ozone selectivity, elevated current efficiency, and long-term operational stability. The existence of these problems hinders the widespread commercial adoption of MEA ozone electrolysis cells. Table 4 summarizes the actual performance of various ozone electrolysis cells in recent years.

3. Anode materials for EOP

The critical aspect of EOP lies in selecting anode materials [2,63], which are essential for the efficiency and stability of the system. The anodic oxidation reaction involves both EOP and OER. By examining equations (1.6) and (1.7), it is evident that OER is a four-electron reaction process, while EOP is a six-electron reaction process. In most cases, the OER process is more favorable and has a clear advantage over the EOP process [64,65]. Fig. 2 compares the reaction potentials of OER and EOP, showing that the anodic reaction in EOP has a higher reaction potential compared to OER. Therefore, a key requirement for EOP anode materials is a relatively high overpotential, promoting the production of ozone over oxygen [50,66,67]. Additionally, as the PEM is in a wet state during the reaction, the system tends to be acidic. Most metals dissolve and passivate at low pH levels [68]. Therefore, anode materials must possess

Table 4
Actual performance of different ozone electrolysis cells.

Ozone electrolysis cell	Anode materials	Electrolyte	Current density	Efficiency	Gaseous O_3	Dissolved O_3	Energy consumption	Stability test	Ref.
Single-chamber	Pt_1/BND	Saturated K_2SO_4	50 mA/cm^2	12.5 %	6.4 ppm	0.24 ppm	/	100 h	[105]
H-type	$Bi_{12}PbO_{20}$-3	Saturated K_2SO_4	50 mA/cm^2	15.1 %	10.8 ppm	8.9 ppm	/	100 h	[77]
H-type	PbO_2/Ta_2O_5	Saturated K_2SO_4	25 mA/cm^2	16.4 %	1.7 ppm	2.7 ppm	/	/	[59]
H-type	7.7-PtZn/Zn-N-C	Saturated K_2SO_4	27 mA/cm^2	4.2 %	1.6 ppm	3.19 ppm	/	20 h	[88]
H-type	PtNi@$B_{13}C_2$-2	Saturated K_2SO_4	50 mA/cm^2	14.8 %	6.0 ppm	3.8 ppm	/	120 h	[90]
H-type	Pt-SAs/BNC-3	Saturated K_2SO_4	50 mA/cm^2	21.0 %	14.7 ppm	/	/	100 h	[89]
H-type	2D ND-1100	Saturated K_2SO_4	50 mA/cm^2	10.0 %	3.6 ppm	7.2 ppm	/	40 h	[102]
MEA	PbO_2 Nanorod	Nafion 117	500 mA/cm^2	14.9 %	222.7 mg/h	/	132.0 Wh/gO_3	50 h	[78]
MEA	Star-like PbO_2	Nafion 212	70 mA/cm^2	7.5 %	/	1.0 ppm	111.6 Wh/gO_3	/	[70]
MEA	Commercial PbO_2	Nafion 212	70 mA/cm^2	4.9 %	/	0.77 ppm	169.7 Wh/gO_3	/	[70]
MEA	PbO_2	Nafion 117	1.5 A /cm^2	18.0 %	/	/	/	/	[73]
MEA	PbO_2	Nafion 117	1.75 A/cm^2	22.6 %	/	/	/	720 h	[75]
MEA	PbO_2 Microsphere	Nafion 117	2.2 A/cm^2	21.7 %	781.2 mg/h	/	/	/	[76]
MEA	F-PbO_2	Nafion 117	2.2 A/cm^2	14.4 %	/	/	/	/	[81]
MEA	Cubic-Pb_3O_4@SiO_2	/	100 mA/cm^2	16.8 %	4.6 ppm	16.9 ppm	/	100 h	[82]
MEA	Pt	Nafion 117	1.59 A/cm^2	23.0 %	/	/	/	50 h	[1]
MEA	SnO_2	Nafion 117	19.2 mA/cm^2	17.0 %	/	0.43 ppm	59.0 Wh/gO_3	/	[31]
MEA	Ni-Sb-SnO_2	Nafion 117	16.9 mA/cm^2	15.2 %	/	19.4 ppm	47.4 Wh/gO_3	/	[51]
MEA	BDD	Nafion N324	/	46.0 %	/	4.6 ppm	143.1 Wh/gO_3	/	[46]
MEA	CVD	Nafion 424	/	36.6 %	/	1.6 ppm	/	20 h	[101]
MEA	HPHT	Nafion 424	/	23.7 %	/	1.2 ppm	/	20 h	[101]
MEA	p-BDD	Nafion 117	200 mA/cm^2		/	4.8 ppm	600 Wh/gO_3	40 h	[103]

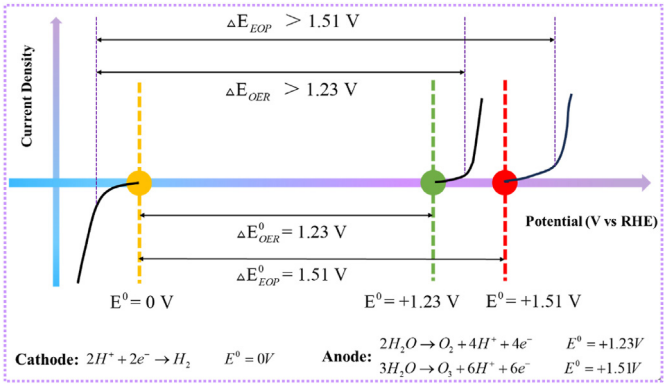

Fig. 2. Schematic diagram of the comparison of OER and EOP reaction potentials.

high chemical stability to withstand corrosion and degradation in acidic environments, thereby enhancing lifespan. This ensures the long-term maintenance of efficient and stable EOP performance, leading to efficient, stable, and sustainable ozone production. Due to the requirement for high oxygen evolution potential and exceptional chemical stability, the selection range of anode materials suitable for EOP is relatively narrow. Presently, research on anode materials with practical applications primarily centers on lead-based catalysts, platinum and its alloys, doped tin dioxide (SnO_2), and BDD electrodes.

3.1. Lead-based catalysts

Lead-based catalysts, one of the earliest anode materials used in EOP, remain popular among many research groups. It offers advantages including high oxygen evolution potential, good chemical stability, and low cost [41,69]. These advantages distinguish it among numerous EOP anode materials, positioning it as one of the most mature materials in the EOP field. However, commercially available lead-based materials often lack crystal type distinction, and key properties such as ozone selectivity, oxygen evolution potential, and corrosion resistance require further improvement. The physical and chemical properties of lead-based catalysts heavily rely on their structure, morphology, and phase composition [70–72]. Studies have demonstrated that lead-based catalysts of various shapes and sizes exhibit diverse practical performances in the EOP process [61,73,74]. Therefore, controlling the nanoscale catalytic structure of lead-based catalysts is an effective approach to enhancing electrocatalytic activity and ozone production efficiency. Researchers have successfully synthesized various leaded nanostructures as anode materials for EOP, achieving satisfactory performance. Fig. 3 illustrates different nanostructured lead-based materials utilized in recent EOP applications.

Wang et al. [71] prepared EOP anode catalysts exhibiting a variety of morphologies by precisely controlling the particle sizes of lead dioxide (PbO_2). Following an extensive 200-hour stability testing evaluation, the PbO_2 catalyst, characterized by its rougher surface morphology, demonstrated enhanced EOP stability. The authors suggested that the increased stability of oxygen radicals on the rougher surface of PbO_2 could be attributed to a more robust interaction with the surface morphology. However, this hypothesis remains speculative, as it is founded solely on two preceding studies, and the current article lacks any experimental characterization or computational analysis to substantiate such a view. The precise underpinning mechanism of this phenomenon has yet to be empirically validated. Chen et al. [75] successfully prepared nanostructured lead dioxide catalysts in nanowire form by electrodeposition using anodic aluminum oxide (AAO) membranes as templates. The catalyst, possessing an average pore size matching that of the AAO membrane, exhibited no notable performance degradation over 30 days of continuous operation in a PEM ozone electrolysis cell, ensuring sustained high EOP performance. Post the 30-day stability test, the authors conducted a basic characterization of the catalyst's morphological changes, neglecting to delve into the changes in the catalyst's current efficiency and ozone production subsequent to the durability test.

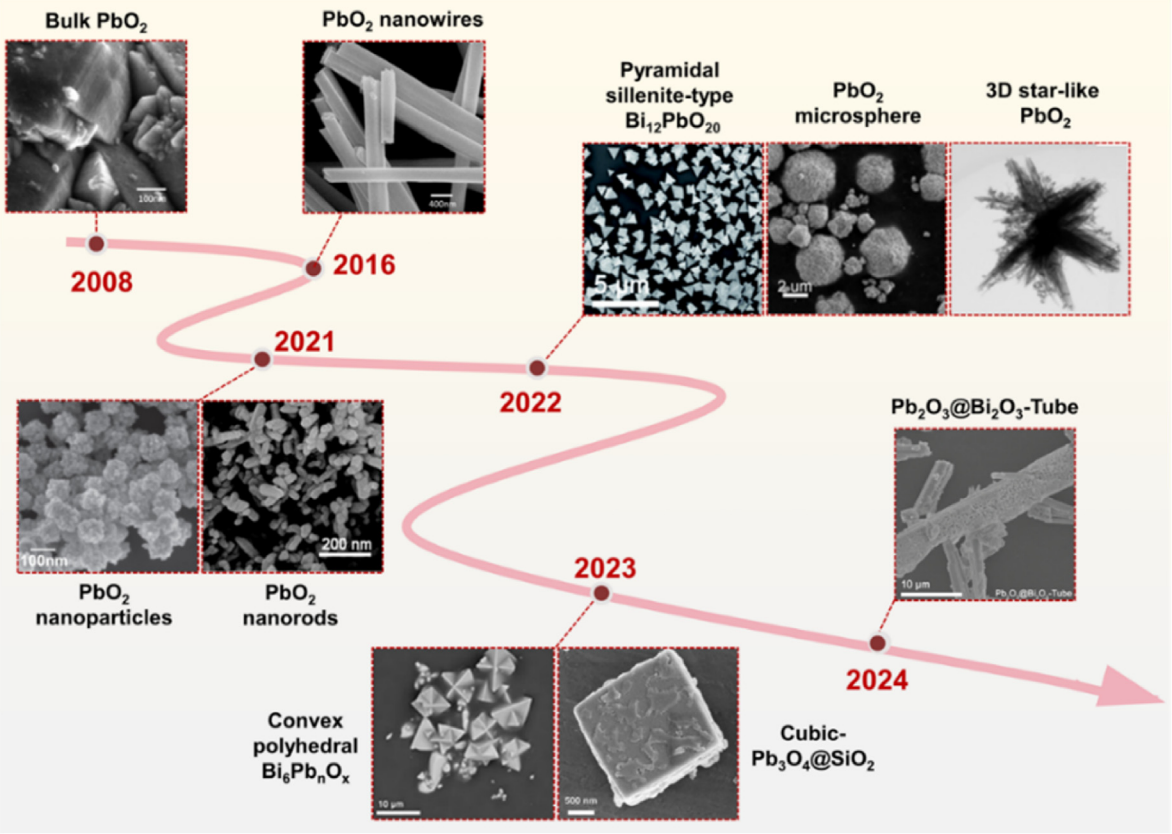

Fig. 3. Summary of different nanostructured lead-based materials, reproduced from Refs. [60,70–72,74–78,82].

Therefore, a comprehensive evaluation of the catalyst's performance degradation over extended periods is imperative for ascertaining its suitability and potential for large-scale industrial utilization. Yu et al. [76] synthesized highly active and uniform spherical lead dioxide catalysts using a one-pot method. This method provides control over the crystal type and particle size of lead dioxide, maintaining a current efficiency of 21 % at high current densities, in contrast to lead dioxide prepared using traditional electrochemical methods. Chemical synthesis enables the preparation of homogeneous lead dioxide catalysts with higher surface area and catalytic activity compared to traditional electrochemical methods. Wang et al. [70] synthesized 3D star-shaped lead dioxide with high EOP catalytic activity using a template-free hydrothermal method. This unique nanostructure exposes catalytic active sites, leading to a significant reduction in EOP energy consumption. From the point of view of EOP performance, the catalytic activity of 3D star catalysts is very limited.

Due to the toxicity of lead, the design of the catalyst structure should adeptly balance the imperative of achieving superior EOP activity with the critical objective of minimizing lead content, thereby significantly alleviating the potential for environmental contamination and adverse health impacts. Shi et al. [77] addressed the high toxicity and poor durability of commercial lead dioxide by developing pyramid-shaped $Bi_{12}PbO_{20}$ with low lead content and reduced toxicity using a hydrothermal method that incorporates Pb into a Bi_2O_3 framework. The introduction of the Bi_2O_3 framework also enhances the durability of the catalyst. The authors attributed the performance enhancement to the weak interaction between Pb and O in the pyramid-shaped $Bi_{12}PbO_{20}$, which reduces the formation energy of oxygen vacancies, promotes lattice oxygen desorption and coupling, and facilitates ozone formation. Jiang et al. [78] prepared nanorod-shaped lead dioxide with different performances by controlling the hydrothermal synthesis temperature, revealing the influence of crystal facets and lattice oxygen on EOP performance and providing theoretical support for enhancing EOP performance. Due to its unique band structure, tantalum oxide has a higher oxygen evolution overpotential. Yan et al. [59] utilized this property to prepare three-dimensional β-PbO_2/Ta_2O_5 nanorods by loading lead dioxide onto Ta_2O_5, where the synergistic effect between lead dioxide and Ta_2O_5 promoted intermediate adsorption, reduced the reaction barrier, and thus enhanced EOP performance. Through the control of lead dioxide nanostructures, lead dioxide anode systems suitable for EOP with better performance, longer durability, and lower toxicity have been developed. Shi et al. [74] fabricated tubular carriers embedded with Pb_2O_3 particles using a wet chemical synthesis method. During EOP, the structure undergoes a dissolution-based restructuring, which creates additional active sites and optimizes the reaction microenvironment. The authors substantiated this hypothesis with comparative assay illustrations, which were meticulously conducted both before and after a short-term EOP reaction. However, the EOP performance of the samples post the 40-hour short-term durability test was not assessed, thus leaving the true durability of the samples unconfirmed.

Researchers have explored various strategies beyond controlling the nanostructure of lead dioxide to enhance catalyst performance. Element doping, a common approach in traditional catalyst preparation [79,80], has been investigated for its effectiveness in improving EOP activity when doping F elements into lead dioxide electrodes [42]. Yu et al. [81] demonstrated the preparation of lead dioxide electrodes doped with various F contents through the addition of NaF solution during electrodeposition, achieving a peak EOP current efficiency of 14.36 %. Through a combination of experimental data and DFT calculations, the authors attribute the performance enhancement to F doping, which suppresses α-PbO_2 formation and boosts oxygen adsorption capacity, as depicted in Fig. 4a and b. Liu et al. [82] developed superhydrophobic cubic Pb_3O_4@SiO_2 by encapsulating homemade superhydrophilic cubic Pb_3O_4 particles with a layer of SiO_2. The incorporation of SiO_2 not only

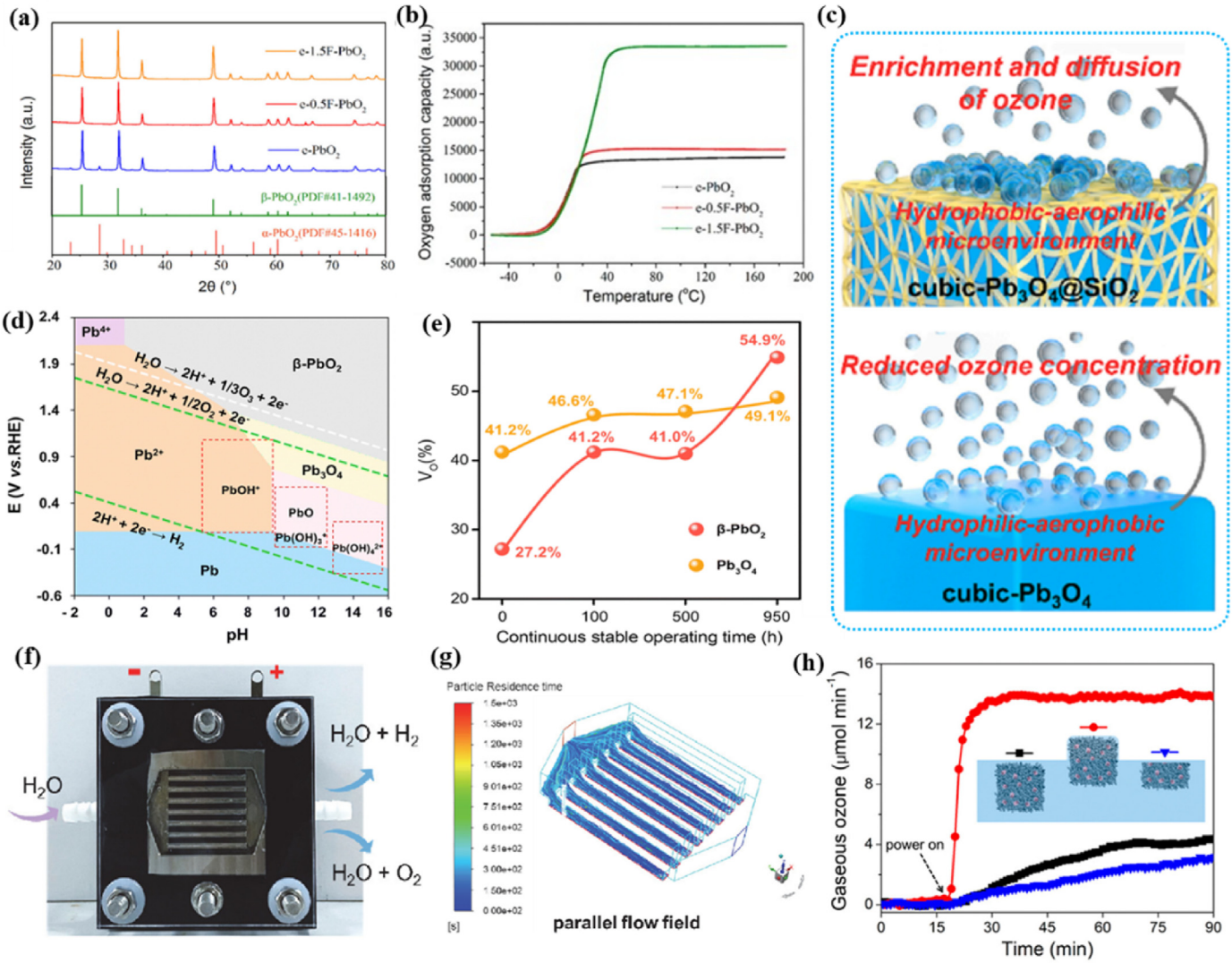

Fig. 4. (a) XRD spectra of e-PbO_2, e−0.5F-PbO_2, and e−1.5F-PbO_2 (b) integration results related to O_2 adsorption capacity, reproduced from Ref. [81] (c) schematic dispersion of bubbles on the surface of cubic-Pb_3O_4@SiO_2 electrode and cubic- Pb_3O_4 electrode, reproduced from Ref. [82] (d) Pourbaix diagram of lead oxide phases under different electric field and pH conditions (e) oxygen vacancy rates (V_O%) on the surfaces of Pb_3O_4 and β-PbO_2 during the EOP process, reproduced from Ref. [83] (f) photograph of transparent EOP electrolysis cell (g) CFD simulation results of bubble trajectories in a parallel flow field, reproduced from Ref. [85] (h) time-course gaseous ozone productivity under varied electrolytic modes as shown in the inset, reproduced from Ref. [86].

enhances the diffusion and oxygen adsorption of active molecules on the electrode, creating a conductive microenvironment for oxygen affinity as shown in Fig. 4c, but also provides system protection, enabling stable EOP operation for 400 hours.

Since the durability of lead-based catalysts under high current density is suboptimal and the current understanding of its mechanism is limited, further research in this aspect is essential. Liu et al. [83] investigated the impact of phase shuttle on Pb_3O_4 during EOP using both *in situ* and *ex situ* characterization techniques. Pb_3O_4 underwent phase shuttle through a lattice oxygen oxidation mechanism, leading to *in situ* reconstruction into β-PbO_2, as shown in Fig. 4d. The appearance of adsorbed oxygen at approximately 531.0 eV is closely associated with the presence of surface oxygen vacancies (V_O) [84]. In prolonged EOP experiments, the authors tracked the orbital changes of Pb_3O_4 and β-PbO_2 using O 1s X-ray photoelectron spectroscopy to monitor the trend of V_O variation in both experimental processes, as illustrated in Fig. 4e. The V_O content on the surface of β-PbO_2 increased by approximately 50 %. During the reconstruction process, there was a slight increase in the V_O content of Pb_3O_4. The results indicate that the reconstructed β-PbO_2 from Pb_3O_4 during EOP has a more stable surface structure, showing higher EOP activity and stability compared to commercial β-PbO_2. The ozone production rate remained stable at 350 mgh^{-1} g^{-1} after 900 hours of operation. To better understand the factors influencing EOP efficiency at high current density, Liu et al. [85] introduced custom square catalysts into a visualization electrolysis cell, as shown in Fig. 4f. They compared the efficiency of reactants and gaseous products in traditional point-like flow fields and parallel flow fields based on anode gas flow rate and Faradaic efficiency. The study concluded that parallel flow fields promote more efficient mass transfer of reactants and gaseous products during EOP. Furthermore, using computational fluid dynamics (CFD) simulation technology, it was demonstrated that bubbles generated on the anode side in the parallel flow field are rapidly transferred as small particles without causing blockages in the channel, as depicted in Fig. 4g. This promotes gas diffusion and facilitates an efficient mass transfer process.

Another method to enhance ozone production involves the suppression of the competing OER reaction. Using an alloying-dealloying technique, Zhang et al. [86] fabricated a bulk porous Pb (BPP) matrix. They then processed to deposit β-PbO_2 onto this matrix in an *in situ* approach, culminating in the fabrication of β-PbO_2@BPP electrodes. In Fig. 4h, the utilization of this porous electrode enabled the rapid production of

gaseous ozone upon activation during the semi-immersion operation phase. Upon reaching equilibrium, the rate of production surpassed that of the fully submerged electrode-based EOP by a factor of more than three. The substantial performance improvement is primarily attributed to the capillary pressure, which enhances the oxygen dissolution in the non-submerged electrode area, thereby significantly inhibiting the desorption of adsorbed oxygen. Consequently, the OER process is effectively suppressed, achieving a Faraday efficiency of approximately 21 % in the production of ozone.

3.2. Platinum and its alloys

Similar to lead-based catalysts, platinum is one of the earliest investigated anode materials for EOP. Platinum exhibits exceptional stability, maintaining prolonged electrochemical activity during ozone production and preserving structural integrity and corrosion resistance in reactions [87]. Additionally, platinum delivers superior EOP performance whether employed as the primary catalyst materials or as a coating on various substrates [66,88–90] owing to its high oxygen evolution potential. However, platinum is costly and entails expenses in large-scale applications as a precious metal. Studies have shown that in traditional polymer electrolyte membrane systems employing platinum electrodes, long-term operation can lead to membrane degradation and pore formation due to interactions with platinum particles, resulting in a significant reduction in ozone generation efficiency [1]. To enhance current efficiency and reduce costs, researchers are exploring alloy design for composite materials or nanostructure optimization to minimize platinum usage.

Yuan et al. [88] selected suitable non-precious metals to modulate Pt and developed PtZn nanoparticles embedded within atomically dispersed Zn-N-C porous carbon matrices, exhibiting size-dependent effects. The synthesis procedure is illustrated in Fig. 5a. Through synergistic effects, atomically dispersed Zn-N-C significantly enhances the electrocatalytic activity of PtZn nanoparticles. Optimization of size-control resulted in a gaseous ozone production rate of 1647 ppb for the catalyst, as depicted in Fig. 5b, notably improving the performance of EOP. However, the performance of the catalyst fluctuated during the 20-hour stability test, which suggests that its activity may diminish over extended periods of operation, thereby necessitating further enhancements to its long-term stability. Gu et al. [89] developed a Pt-SAs/BNC catalyst by embedding atomic platinum into BNC nanotubes, establishing a local environment rich in oxygen intermediates. The Pt-SAs/BNC-3 catalyst exhibited a Faradaic efficiency exceeding 20 %, as shown in Fig. 5c, while maintaining excellent stability during a 100-hour operating period (Fig. 5d), presenting a novel approach for producing highly active, environmentally friendly EOP catalysts. Alloying for component diversification is a crucial strategy in optimizing Pt-based electrocatalysts. Li et al. [90] designed and synthesized PtNi alloys encapsulated in $B_{13}C_2$. DFT calculations revealed that the distance between B atoms on $B_{13}C_2$ is similar to the bond length of ozone, promoting pentagonal ring structure formation. The adsorption model is depicted in Fig. 5e. The synergistic interaction between PtNi and $B_{13}C_2$ promotes pentagonal ring structure formation. Adsorption energy analysis showed that ozone molecules can stably adsorb on the $B_{13}C_2$ (012) surface, and the addition of PtNi effectively weakened the adsorption of ozone on $B_{13}C_2$, as illustrated in Fig. 5f, promoting ozone desorption.

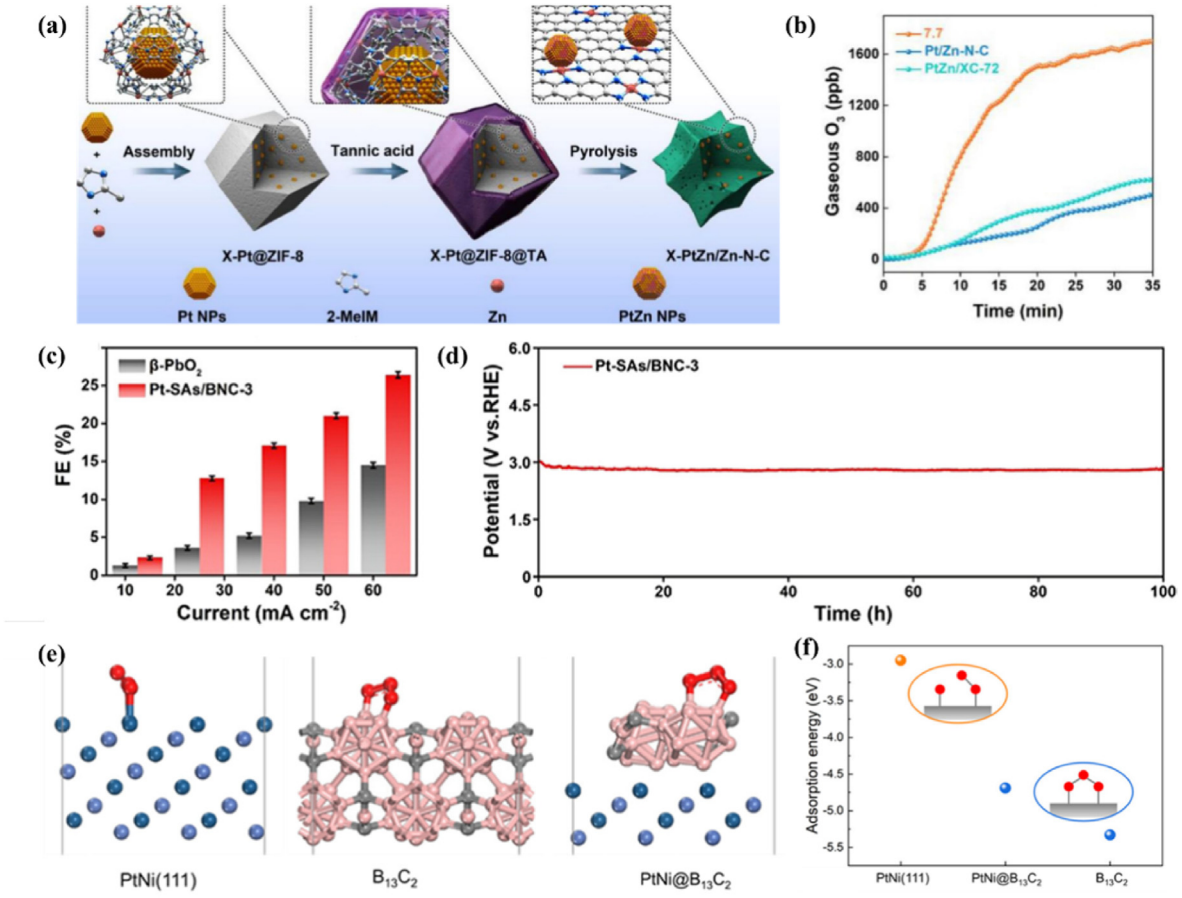

Fig. 5. (a) Schematic illustration of the synthesis route for X-PtZn/Zn-N-C electrocatalysts (b) gaseous ozone production rates of 7.7-PtZn/Zn-N-C, Pt/Zn-N-C, and PtZn/XC-72 at a current density of 50 mA cm^{-2}, reproduced from Ref. [88] (c) Faradaic efficiency of Pt-SAs/BNC-3 and commercial β-PbO_2 at different current densities (d) stability of Pt-SAs/BNC-3 at a constant potential of 3V, reproduced from Ref. [89] (e) structural optimization and charge density difference of ozone adsorption on PtNi(111), $B_{13}C_2$, and PtNi@ $B_{13}C_2$ (f) surface adsorption energy of ozone on PtNi(111), $B_{13}C_2$, and PtNi@ $B_{13}C_2$, reproduced from Ref. [90].

3.3. Doped SnO_2

Doped SnO_2 is a non-toxic semiconductor material with a high oxygen evolution potential, offering distinct advantages over toxic lead-based catalysts and costly platinum. Studies indicate that adsorbed *OH species on the electrode surface could act as vital activation intermediates in the EOP process, and doped SnO_2 electrodes generate a large quantity of adsorbed *OH, thereby significantly improving ozone generation efficiency during electrolysis [59]. Recent research has focused on incorporating different elemental dopants into SnO_2 to address the inherent instability SnO_2, resulting in enhanced ozone production efficiency at elevated current densities. Cheng et al. [91] initially conducted electrolysis experiments using Sb-doped SnO_2 electrodes in $HClO_4$ solution, achieving an EOP current efficiency of 15 %. Subsequently, Wang et al. [92] found that the performance of SnO_2 is also influenced by trace secondary doping, investigating the impact of adding Ni to Sb-doped SnO_2 on ozone production. They determined that at a Ni: Sb: Sn ratio of 1:8:500, the highest current efficiency reached 36.3 %. This suggests that even a small amount of Ni doping can significantly influence the activity for ozone synthesis on Sb-SnO_2 electrodes. Christensen et al. [93] further optimized the ratios of Sn:Sb:Ni and cell potential. Through analyzing the change in minimum current efficiency based on Ni content, they identified a Ni: Sb: Sn ratio of 3:8:500 that can achieve 50 % current efficiency at room temperature with 2.7 V.

Besides doping element ratios, controlling the catalyst structure can enhance performance. Wang et al. [94] synthesized SnO with different exposed surfaces by adjusting the crystal face microenvironments. As shown in Fig. 6a, among the tested electrocatalysts, SnO-1 exhibits the highest overpotential of 2.77 V at a current density of 10 mA cm^{-2}, indicating superior ozone generation potential. Fig. 6b illustrates the percentage of (110) and (002) crystalline surfaces for different samples, revealing that SnO-1 possesses a higher percentage of (110) crystalline surfaces, leading to the best EOP performance and Faraday efficiency of 22.0 %. This enhancement is attributed to the robust adsorption of

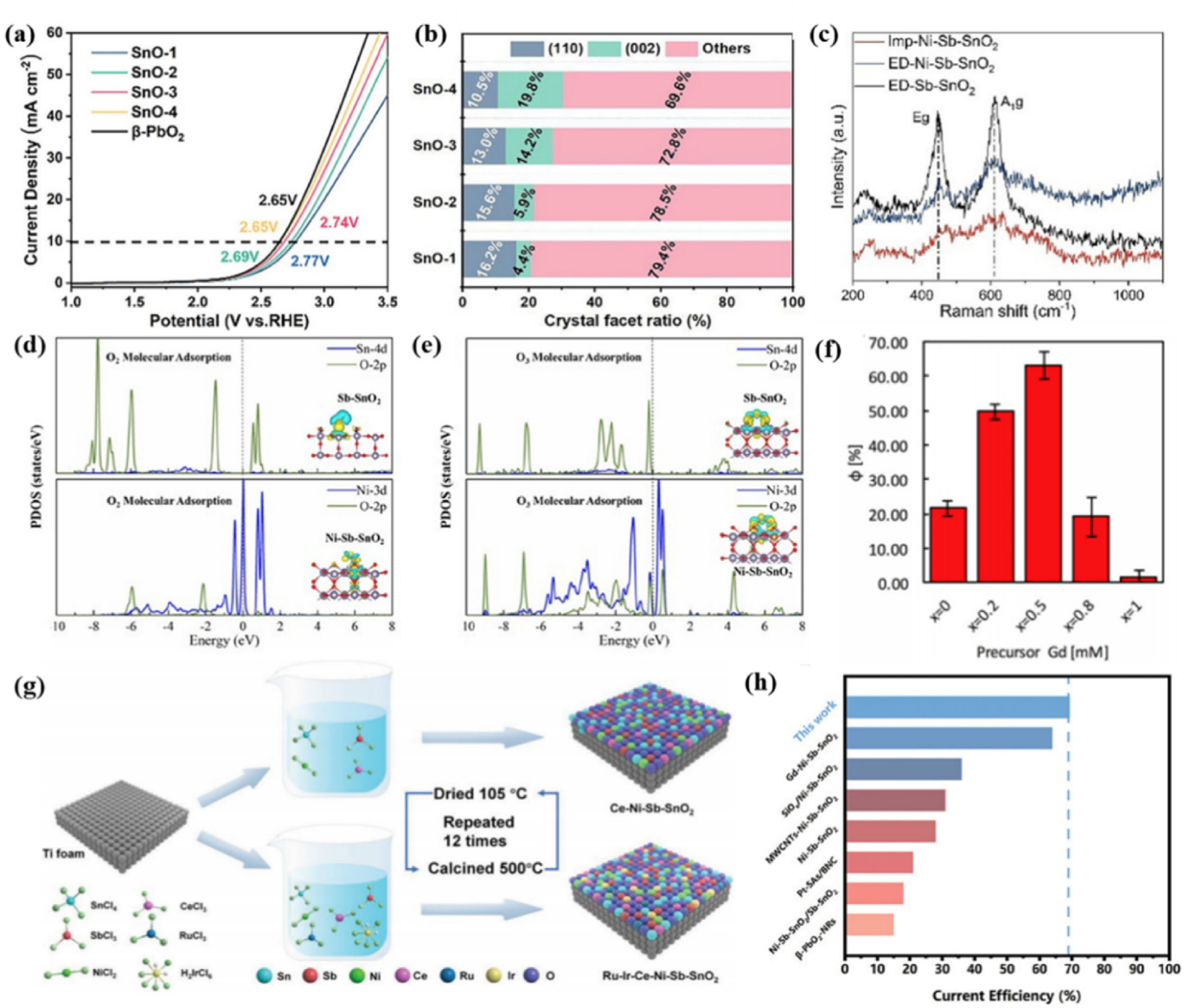

Fig. 6. (a) Steady-state polarization curves of SnO-n (n = 1, 2, 3, 4) and β-PbO_2 (b) calculated peak heights from XRD spectra for (110) and (002) crystal planes, reproduced from Ref. [94] (c) Raman spectra of Imp-Ni-Sb-SnO_2, ED-Ni-Sb-SnO_2, and ED-Sb-SnO_2 (d) adsorption of oxygen on the surfaces of Sb-SnO_2 and Ni-Sb-SnO_2 (e) adsorption of ozone on the surfaces of Sb-SnO_2 and Ni-Sb-SnO_2, reproduced from Ref. [95] (f) influence of Gd and Ni doping ratios on the faraday efficiency of the EOP method, reproduced from Ref. [98] (g) schematic diagrams illustrating the preparation methods of Ce-Ni-Sb-SnO_2 and Ru-Ir-Ce-Ni-Sb-SnO_2, reproduced from Ref. [99] (h) comparison of current efficiency between $Cu_{1.45}$Ni-ATO and recently reported EOP electrodes, reproduced from Ref. [100].

intermediate species such as O* and O_2* on the (110) surface, promoting ozone formation. Ding et al. [95] enhanced EOP selectivity by adjusting the surface Ni active sites and oxygen vacancy defect content of Ni-Sb-SnO_2 electrocatalysts. As shown in Fig. 6c, Raman spectra of various samples indicate a gradual decrease in peak intensity and an increase in half-peak width for the A_{1g} and E_g modes of SnO_2, indicating an increase in lattice defects and oxygen vacancies, which leads to a reduction in lattice space symmetry. Previous studies have demonstrated that an increase in peroxide vacancies is favorable for ozone generation [96]. The authors also investigated the influence of different electronic states of Ni and Sn on oxygen/ozone adsorption behavior. Fig. 6d demonstrates that effective oxygen chemical adsorption only occurred on Ni-modified surfaces. In the Ni-Sb-SnO_2 model, after ozone adsorption, the corresponding projected density of states displayed strong hybrid electronic states near the Fermi level as demonstrated in Fig. 6e. Electron transfer from Ni sites to ozone molecules into the π* orbitals led to conjugation, ultimately forming stable pentagonal ring adsorption configurations. Essentially, the Ni sites on the Ni-Sb-SnO_2 surface serve as potential trapping sites for oxygen/ozone molecules.

Ni and Sb co-doped SnO_2 has also been used to modify titanium-based electrodes. AliBenvidi et al. [97] prepared different titanium-based electrodes for the EOP process using spin-coating and thermal decomposition methods and incorporated multi-walled carbon nanotubes in mixed metal oxide composites. The study showed that maintaining the molar ratio of Sn/Sb/Ni at 500:8:1 and increasing multi-walled carbon nanotubes improved ozone generation efficiency. All modified titanium electrodes modified with SnO_2 materials generated ozone concentrations exceeding 5 mg L^{-1}. Despite the high current efficiency of Ni and Sb co-doped SnO_2 electrocatalysts, their catalytic activity and selectivity remain inadequate for commercial use. To further enhance ozone generation efficiency, James L. Lansing et al. [98] identified active dopants other than Ni. Adding Gd to Ni-Sb-SnO_2 increased ozone selectivity threefold compared to Ni doping alone, achieving a Faradaic efficiency of 64 % as shown in Fig. 6f. The inclusion of Gd not only inhibited oxygen evolution but also enhanced the rate of ozone production. Xue et al. [99] introduced the lanthanide metal Ce into Ni-Sb-SnO_2 oxides to construct Ce-Ni-Sb-SnO_2 quaternary metal oxides, as shown in Fig. 6g. Multi-component oxides can modulate the three-dimensional orbital electronic structure by interacting with metal elements, optimizing the adsorption free energy of oxygen intermediates to enhance EOP performance, achieving a remarkable Faradaic efficiency of 43.9 %. Jin et al. [100] further doped Cu atoms into Ni and Sb co-doped SnO_2, surpassing a current efficiency exceeding 70 % compared to recently published catalysts in Fig. 6h. The inclusion of Cu atoms had a positive impact on both EOP performance and durability. DFT calculations also indicated that the improved electronic structure post Cu doping contributed to the enhanced electrochemical performance. The weak bond between oxygen and active sites allowed the effective desorption of O* and O_2*, promoting the formation of ozone and enhancing the selectivity of Cu, Ni, and Sb co-doped SnO_2 for EOP.

The selection of dopants for SnO_2 is crucial. The high oxygen precipitation potential of SnO_2, coupled with its abundant surface oxygen vacancy structure, forms the foundation for achieving higher efficiency. Despite these advantages, SnO_2's EOP selectivity remains inadequate, necessitating improvements in both electrical conductivity and chemical stability. In the process of elemental doping, a priority is to incorporate elements that enhance electrical conductivity, with Ni being the most frequently utilized. In addition, the incorporation of elements that bolster EOP selectivity is essential, typically involving the addition of transition metal ions to stimulate active intermediates and oxygen vacancies, with Sb being the most prevalent. Looking ahead to the subsequent development, the optimization of SnO_2-based doped catalysts can be pursued through a multifaceted approach. Firstly, in addition to Ni and Sb, the exploration of doping with additional transition metals or rare earth elements, such as Fe, Co and Ce, could be instrumental in modulating the electronic structure of SnO_2, thereby promoting the generation of active sites on the catalyst surface and improving both EOP selectivity and catalytic activity. Moreover, considering the adsorption and activation processes of reactants during the electrochemical reactions, future investigations might explore strategies for enhancing the catalyst's affinity and selectivity towards ozone generation, achieved through the optimization of surface structures and the manipulation of crystal defects.

3.4. BDD

Due to its stable sp^3 structure, high electrochemical stability, and wide potential window, BDD electrodes are excellent and ideal anode materials for EOP [46]. Boron, a third main group element with three electrons in its outer shell, possesses a deficit electron structure. Boron doping provides extra charge carriers to diamond electrodes, thereby enhancing the conductivity of semiconductor diamond [41]. Due to the high cost of standalone diamond film, BDD electrodes are typically deposited on suitable substrates using chemical vapor deposition (CVD) on materials Si, Ti, Ta, Mo, and glassy carbon [41]. Wood et al. [101] explored the electrode fabrication using diamond particles synthesized through the high-pressure high-temperature (HPHT) method, compacted under high pressure and temperature as shown in Fig. 7a. Since HPHT growth often results in diamond containing 100 ppm of singly substituted nitrogen, AlB_2 was utilized as a boron source to mitigate boron-nitrogen charge compensation. Experimental results revealed a roughly 30 % decrease in ozone production rate with HPHT BDD electrodes compared to those grown via CVD as demonstrated in Fig. 7b, while showcasing feasibility and potential in the EOP process. Despite the inherent intricacies associated with the HTHP process and the comparatively diminished efficiency of the EOP, it remains evident that these characteristics significantly contrast with those of BDD prepared via conventional CVD methods, thereby necessitating further advancements in the technology to bridge these disparities.

To improve the ozone generation efficiency of BDD electrodes, Arihara et al. [46] optimized the design of standalone perforated BDD electrodes by adjusting pore number, pore size, and electrode thickness. They discovered that increasing the number of pores per unit area was the most effective method to improve current efficiency. The best perforation setup included a thickness of 0.5–0.6 mm and a maximum pore diameter of 1 mm per unit area. Following electrode optimization, a current efficiency of 47 % was achieved with a thickness of 0.54 mm and 312 perforations. Generally, enhancing the adsorption capacity for oxygen and electrochemically active surface area of BDD electrodes is crucial for achieving high ozone generation performance due to the typically weak adsorption of oxygen-containing substances and limited chemical sites on the BDD surface. The surface properties of diamond anodes in the EOP process remain incompletely understood. Yang et al. [102] conducted an in-depth study on hybrid 2D diamond nanosheets with variable sp^3/sp^2 ratios. As shown in Fig. 7c, the sp^3/sp^2 carbon content in hybrid 2D ND was determined using X-ray photoelectron spectroscopy, and the adsorption energy of oxygen/ozone on the 2D ND surface at different sp^3/sp^2 ratios was calculated through DFT calculations. Ratios of 5:4, 6:3, and 7:2 corresponded to the reaction regions where selective ozone generation occurred, as shown in Fig. 7d. At the cell voltage of 3.5 V vs. RHE, 2D ND-1100 exhibited the highest concentration of dissolved ozone, surpassing hybrid 2D ND electrocatalysts, as illustrated in Fig. 7e.

As shown in Fig. 7f, Liu et al. [103] employed oxygen plasma etching technology to fabricate porous BDD (p-BDD) electrodes, introducing oxygen functional groups on the BDD surface to enhance its hydrophilicity and increase the electrode's specific surface area. Compared to bare BDD, the ozone generation capacity of p-BDD increased by 1.39 times, with a unit consumption of only 39.65 %. Furthermore, p-BDD exhibited excellent stability during long-term water electrolysis, showing a mere 4.2 % decrease in current density over 40 h, as shown in Fig. 7g. Nishiki et al. [104] used tap water, a more accessible and cost-effective alternative to pure water, to evaluate the universality of BDD electrodes. Although the current efficiency decreased by 1/2∼1/3 compared to

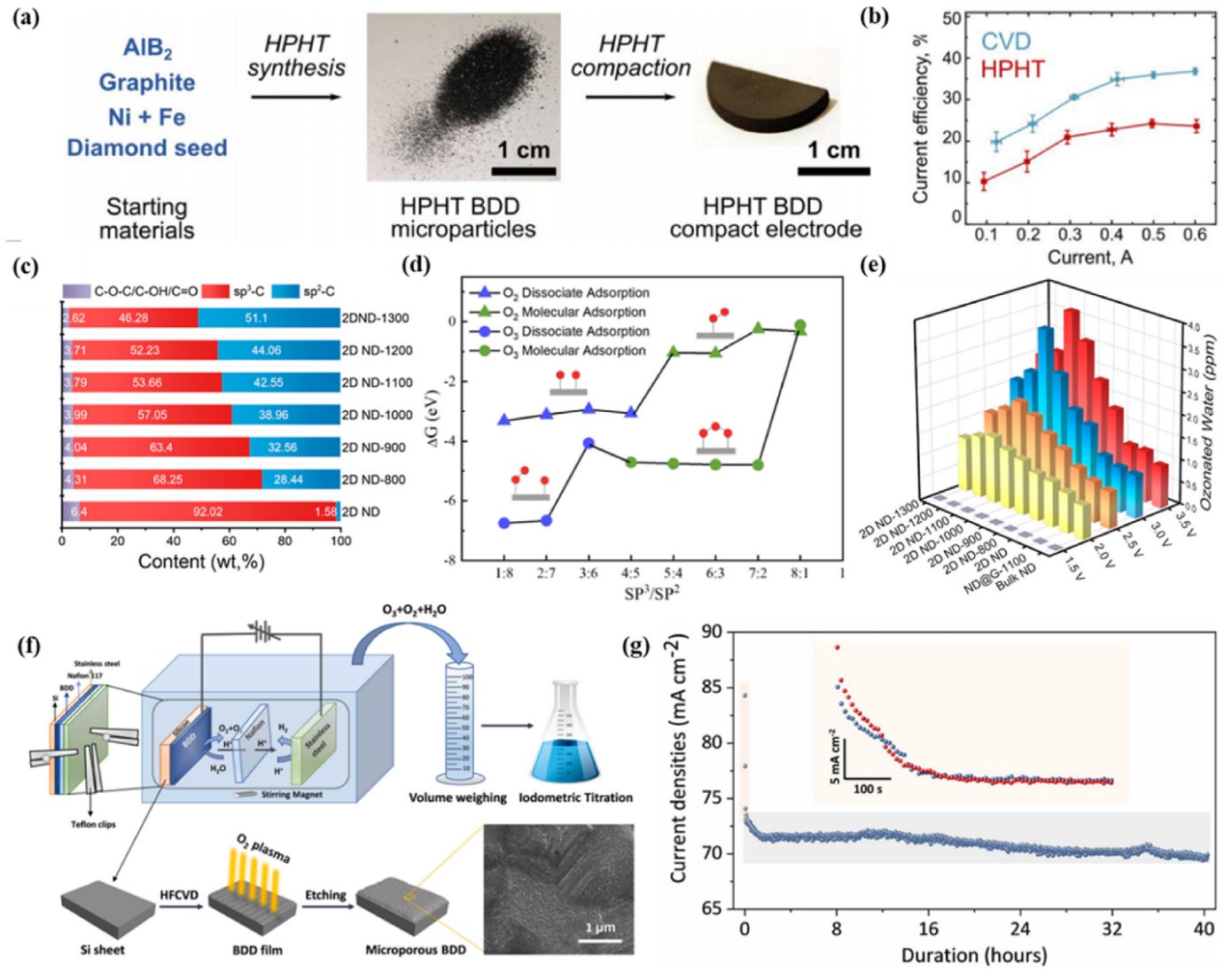

Fig. 7. (a) Schematic representation of the fabrication steps for HPHT BDD electrodes (b) relationship between current efficiency and applied current (n = 3), reproduced from Ref. [101] (c) relative content of sp^3-C and sp^2-C in 2D ND-X (d) adsorption energy of oxygen and ozone on the surface of 2D ND under different sp^3/sp^2 ratios (e) dissolved ozone concentration of 2D ND-X, 2D ND, Bulk ND, and ND@G-1100 at different voltages, reproduced from Ref. [102] (f) experimental setup, quantification method of dissolved ozone concentration in water, preparation process of microporous BDD, and SEM image of microporous BDD (g) long-term stability test of ozone generation on p-BDD, reproduced from Ref. [103].

using pure water, the electrode exhibited good stability. Ozone production remained unaffected when the chloride ion concentration was below 50 mg L^{-1}, and the ozone-dissolved water produced by the device passed the sterilization test. Lu et al. [105] introduced an innovative approach using atomically dispersed Pt with boron and nitrogen co-doped two--dimensional BDD films to achieve efficient electrochemical production of ozone and hydrogen peroxide. This synergistic design enhances the activity and stability of the catalyst, showing a robust potential for practical applications. However, the synthesis of single-atom Pt remains a complex and costly process, necessitating further research to improve the catalyst's structural stability and industrial viability.

At present, the mainly EOP catalyst that has been commercialized on a small scale is BDD, with BDD electrodes prepared via CVD being integrated into a select few small-scale water purification systems [106,107]. These compact water treatment systems demonstrate remarkable efficacy by utilizing BDD electrodes to generate ozone, a substance that is adept at effectively removing organic pollutants and microorganisms from water. The on-demand production of ozone in these systems eliminates the need for large-scale industrial setups, allowing for strategic application in specific steps of the water treatment process. However, to broaden the scope of its applications, additional optimization regarding the robustness and treatment efficacy of these systems is imperative.

4. Conclusion and perspective

Ozone, renowned for its eco-friendliness and efficiency, faces storage challenges and is prone to decomposition at room temperature, rendering on-site generation a more viable option. In this context, the paper presents a comprehensive review of EOP. The paper concisely explains the EOP mechanism and evaluates various types of ozone electrolysis cells, particularly highlighting the developmental benefits of MEA ozone electrolysis cells for ozone production. From the perspective of device optimization, it is expected that the enhancement of the structural integrity of MEAs is anticipated to enhance the efficiency and output of the EOP process, a result achieved by not only expanding the electrode surface area but also by refining the dynamics of mass transfer. Meanwhile, the pursuit of a more efficient integration of the system can improve operational efficiency, thereby reducing both maintenance and

operating expenditures. Finally, the study comprehensively investigates how the choice of anode materials influences electrocatalytic activity and ozone production efficiency, thereby enhancing EOP performance.

Given the growing demand for sustainable and cost-effective ozone production, the optimization of anode materials plays a critical role in improving the overall efficiency and feasibility of EOP systems. Lead-based catalysts, despite their rapid development and relatively mature technology, cannot escape scrutiny due to their inherent toxicity and instability. Future research endeavors will focus on reducing lead content and enhancing stability. Platinum, recognized as an exemplary catalyst in EOP, is in high demand, but its cost implications hinder its widespread commercialization. Innovative strategies to reduce platinum usage or find suitable substitutes are essential to improve both the economic and environmental sustainability of EOP systems. Anodes, such as those composed of doped SnO_2, have demonstrated current efficiencies exceeding 50 % under mild experimental conditions. However, their short lifespans act as a barrier to further advancement, making the enhancement of such anodes' durability a crucial research priority. BDD, the EOP catalyst that has been commercialized on a small scale, boasts commendable electrolysis efficiency and stability to match the needs of small-scale water purification facilities. However, managing costs is a pivotal concern for the development of BDD to facilitate its expansion into large-scale production. This review systematically elucidates the applications of anode materials, including lead-based catalysts, platinum and its alloys, doped SnO_2, and BDD, along with improvement strategies in EOP, with the aspiration to act as a compass for future advancement of anode materials. In summary, the future trajectory of EOP largely depends on overcoming the existing material and cost-related barriers, thereby unlocking its potential for broader industrial and environmental applications.

The development of anode materials for EOP is significantly hindered by the competing OER. The comparatively lower reaction potential of the OER substantially constrains ozone production, thereby posing a critical barrier to the commercialization of EOP technologies. Moreover, the elusive goal of achieving a complete breakthrough in the selectivity of ozone production continues to impact the overall efficiency and viability of the system. In particular, understanding the intricate interplay between anode materials and reaction conditions could hold the key to improving selectivity. Despite the superior performance of precious metal-doped oxides in EOP, their high cost remains a limiting factor for manufacturing and widespread implementation. The introduction of numerous novel materials has broadened the range of EOP anode materials beyond the conventional categories in the literature. For instance, the transition metal oxide niobium pentoxide (Nb_2O_5), renowned for its elevated electrochemical activity, exhibits promising potential in EOP applications [108]. This particular material offers a cost-effective and eco-friendly option, thereby expanding the array of experimental approaches accessible to researchers. Furthermore, leveraging theoretical calculations to explore the reaction mechanisms of EOP materials is a feasible strategy for guiding the development of new, more efficient materials. The employment of advanced modeling techniques could accelerate the identification of innovative materials with superior performance characteristics, consequently diminishing the reliance on trial-and-error methodologies in experimental research. Building on these research advancements, the large-scale commercialization of EOP technology is anticipated to exceed expectations. This technology is poised to not only enhance ozone production but also play a pivotal role in addressing global environmental and energy challenges. Consequently, ongoing exploration and innovation in EOP anode materials offer a promising and impactful direction for future research endeavors.

Declaration of competing interest

The authors declare that they have no known competing financial interests or personal relationships that could have appeared to influence the work reported in this paper.

Acknowledgements

This research was financially supported by the National Natural Science Foundation of China (No. 22208376), Qingdao New Energy Shandong Laboratory Open Project (QNESL OP 202303), Shandong Provincial Natural Science Foundation (No. ZR2024QB175, No. ZR2023LFG005), Taishan Scholar Project (ts201712020). S.L, Y.D. and Y.L acknowledge the support from Science and Technology Innovation Teams of Shanxi Province (202304051001023).

References

[1] F. Okada, K. Naya, Highly efficient and long-lifetime ozone water production system realized using a felt separator, J. Electrochem. Soc. 156 (2009) E125–E131, https://doi.org/10.1149/1.3134544.
[2] K. Naya, F. Okada, Effects of NaCl and Na_2SO_4 cathode electrolytes on electrochemical ozone production, Electrochim. Acta 78 (2012) 495–501, https://doi.org/10.1016/j.electacta.2012.06.071.
[3] M. Rodriguez-Pena, J.A. Barrios Perez, J. Llanos, C. Saez, M.A. Rodrigo, C.E. Barrera-Diaz, New insights about the electrochemical production of ozone, Curr. Opin. Electrochem. 27 (2021) 100697, https://doi.org/10.1016/j.coelec.2021.100697.
[4] Y. Zhou, Worldwide carbon neutrality transition? Energy efficiency, renewable, carbon trading and advanced energy policies, Energy Rev. 2 (2023) 100026, https://doi.org/10.1016/j.enrev.2023.100026.
[5] W.K. Hussam, E.M. Barhoumi, M. Abdul-Niby, G.J. Sheard, Techno-economic analysis and optimization of hydrogen production from renewable hybrid energy systems: Shagaya renewable power plant-Kuwait, Int. J. Hydrogen Energy 58 (2024) 56–68, https://doi.org/10.1016/j.ijhydene.2024.01.153.
[6] S.-H. Lee, Y. Kwon, S. Kim, J. Yun, E. Kim, G. Jang, Y. Song, B.S. Kim, C.-S. Oh, Y.-H. Choa, J.-Y. Kim, J.H. Park, D.-W. Jeong, A novel water electrolysis hydrogen production system powered by a renewable hydrovoltaic power generator, Chem. Eng. J. 495 (2024) 153411, https://doi.org/10.1016/j.cej.2024.153411.
[7] S.O. Ganiyu, C.A. Martínez-Huitle, The use of renewable energies driving electrochemical technologies for environmental applications, Curr. Opin. Electrochem. 22 (2020) 211–220, https://doi.org/10.1016/j.coelec.2020.07.007.
[8] L.A.B. Mascarenhas, F.O. Oliveira, E.S. da Silva, L.M.C. dos Santos, L. de Alencar Pereira Rodrigues, P.R.F. Neves, A.Á.B. Santos, G.A.F. Moreira, G.M. Lobato, C. Nascimento, M. Gerhardt, B.A.S. Machado, Technological advances in ozone and ozonized water spray disinfection devices, Appl. Sci. 11 (2021) 3081, https://doi.org/10.3390/app11073081.
[9] W. Ding, W. Jin, S. Cao, X. Zhou, C. Wang, Q. Jiang, H. Huang, R. Tu, S.-F. Han, Q. Wang, Ozone disinfection of chlorine-resistant bacteria in drinking water, Water Res. 160 (2019) 339–349, https://doi.org/10.1016/j.watres.2019.05.014.
[10] K. Rangel, F.O. Cabral, G.C. Lechuga, J.P.R.S. Carvalho, M.H.S. Villas-Bôas, V. Midlej, S.G. De-Simone, Potent activity of a high concentration of chemical ozone against antibiotic-resistant bacteria, Molecules 27 (2022) 3998, https://doi.org/10.3390/molecules27133998.
[11] Z. Xia, L. Hu, Treatment of organics contaminated wastewater by ozone micro-nano-bubbles, Water 11 (2018) 55, https://doi.org/10.3390/w11010055.
[12] K. Yang, J. Yu, Q. Guo, C. Wang, M. Yang, Y. Zhang, P. Xia, D. Zhang, Z. Yu, Comparison of micropollutants' removal performance between pre-ozonation and post-ozonation using a pilot study, Water Res. 111 (2017) 147–153, https://doi.org/10.1016/j.watres.2016.12.043.
[13] H. Yuan, C. Zhan, H. Xia, W. Xiaomao, W. Xianghua, A novel catalytic membrane integrated with ozone process for secondary wastewater treatment: Micropollutant removal, membrane fouling control, and its mechanisms, Desalination 565 (2023) 116869, https://doi.org/10.1016/j.desal.2023.116869.
[14] H. Jiang, X. Xu, R. Zhang, J. Chen, Y. Wang, Y. Zhang, F. Yang, A novel combined treatment for pyridine waste gas using liquid absorption, catalytic ozonation, and sulfur autotrophic denitrification (LA-CO-SAD), Chem. Eng. J. 400 (2020) 125997, https://doi.org/10.1016/j.cej.2020.125997.
[15] A.G. Sarah, B.S. Rajanikanth, Nox reduction from biodiesel exhaust by plasma induced ozone injection supported by lignite waste adsorption, IEEE Trans. Dielectr. Electr. Insul. 23 (2016) 1–9, https://doi.org/10.1109/TDEI.2016.7556472.
[16] A.J. Brodowska, A. Nowak, K. Śmigielski, Ozone in the food industry: Principles of ozone treatment, mechanisms of action, and applications: an overview, Crit. Rev. Food Sci. Nutr. 58 (2017) 2176–2201, https://doi.org/10.1080/10408398.2017.1308313.
[17] E.I. Epelle, A. Macfarlane, M. Cusack, A. Burns, B. Thissera, W. Mackay, M.E. Rateb, M. Yaseen, Bacterial and fungal disinfection via ozonation in air, J. Microbiol. Methods 194 (2022) 106431, https://doi.org/10.1016/j.mimet.2022.106431.
[18] R. Pandiselvam, S. Sunoj, M.R. Manikantan, A. Kothakota, K.B. Hebbar, Application and kinetics of ozone in food preservation, Ozone Sci. Eng. 39 (2016) 115–126, https://doi.org/10.1080/01919512.2016.1268947.
[19] D. Lancet, I. Pecht, Spectroscopic and immunochemical studies with nitrobenzoxadiazolealanine, a fluorescent dinitrophenyl analog, Biochemistry 16 (1977) 5150–5157, https://doi.org/10.1021/bi00642a031.

[20] V.K. Sharma, Oxidative transformations of environmental pharmaceuticals by Cl_2, ClO_2, O_3, and Fe(VI): kinetics assessment, Chemosphere 73 (2008) 1379–1386, https://doi.org/10.1016/j.chemosphere.2008.08.033.

[21] F.P. Chee, N.S. Zainuddin, H.L. Ha, J. Dayou, Analysis and characterization of enhanced kinetic reaction on ozone generation using negative corona discharge, J. Phys. Commun. 4 (2020) 075022, https://doi.org/10.1088/2399-6528/ab9fac.

[22] L.G. De Sousa, D.V. Franco, L.M. Da Silva, Electrochemical ozone production using electrolyte-free water for environmental applications, J. Environ. Chem. Eng. 4 (2016) 418–427, https://doi.org/10.1016/j.jece.2015.11.042.

[23] U. Kogelschatz, Dielectric-barrier discharges: their history, discharge physics, and industrial applications, Plasma Chem. Plasma Process. 23 (2003) 1–46, https://doi.org/10.1023/A:1022470901385.

[24] S. Paolo, W. Alexander, S. Alex, I. Felipe, B. Hemaka, A.B. Carlo, N. Gabriele, Influence of the voltage waveform's shape and on-time duration on the dissolved ozone produced by a DBD bubble reactor, Plasma Sources Sci. Technol. 28 (2019) 035001, https://doi.org/10.1088/1361-6595/ab024f.

[25] B. Eliasson, U. Kogelschatz, Modeling and applications of silent discharge plasmas, IEEE Trans. Plasma Sci. 19 (1991) 309–323, https://doi.org/10.1109/27.106829.

[26] B. Eliasson, M. Hirth, U. Kogelschatz, Ozone synthesis from oxygen in dielectric barrier discharges, J. Phys. D Appl. Phys. 20 (1987) 1421–1437, https://doi.org/10.1088/0022-3727/20/11/010.

[27] Y. Zhang, L. Wei, X. Liang, M. Šimek, Ozone production in coaxial DBD using an amplitude-modulated AC power supply in air, Ozone Sci. Eng. 41 (2019) 437–447, https://doi.org/10.1080/01919512.2019.1565986.

[28] K. Nassour, M. Brahami, S. Nemmich, N. Hammadi, N. Zouzou, A. Tilmatine, New hybrid surface–Volume dielectric barrier discharge reactor for ozone generation, IEEE Trans. Ind. Appl. 53 (2017) 2477–2484, https://doi.org/10.1109/tia.2017.2675978.

[29] S. Jodzis, J. Petryk, Gas temperature in an ozonizer. The computer modeling of an actual discharge system, IEEE Trans. Plasma Sci. 39 (2011) 2120–2121, https://doi.org/10.1109/tps.2011.2158559.

[30] P. Liu, Y. Song, Z. Zhang, A novel dielectric barrier discharge (DBD) reactor with streamer and glow corona discharge for improved ozone generation at atmospheric pressure, Micromachines 12 (2021) 1287, https://doi.org/10.3390/mi12111287.

[31] Y. Cui, Y. Wang, B. Wang, H. Zhou, K.-Y. Chan, X.-Y. Li, Electrochemical generation of ozone in a membrane electrode assembly cell with convective flow, J. Electrochem. Soc. 156 (2009) E75, https://doi.org/10.1149/1.3072686.

[32] J. Kitayama, M. Kuzumoto, Analysis of ozone generation from air in silent discharge, J. Phys. D Appl. Phys. 32 (1999) 3032, https://doi.org/10.1088/0022-3727/32/23/309.

[33] S.J.O.S. Jodzis, Effect of silica packing on ozone synthesis from oxygen-nitrogen mixtures, Ozone Sci. Eng. 25 (2003) 63–72, https://doi.org/10.1080/713610651.

[34] H. Claus, Ozone generation by ultraviolet lamps, Photochem. Photobiol. 97 (2021) 471–476, https://doi.org/10.1111/php.13391.

[35] A.W. Ewell, Recent ozone investigations, J. Appl. Phys. 17 (1946) 908–911, https://doi.org/10.1063/1.1707663.

[36] X. Feng, X. Feng, F. Zhang, Enhanced photoelectrochemical oxidation of glycerol to dihydroxyacetone coupled with hydrogen generation via accelerative middle hydroxyl dehydrogenation over a Bi^0/Bi^{3+} interface of a cascade heterostructure, J. Mater. Chem. A 11 (2023) 20242–20253, https://doi.org/10.1039/D3TA04326F.

[37] D. Liu, J.-C. Liu, W. Cai, J. Ma, H.B. Yang, H. Xiao, J. Li, Y. Xiong, Y. Huang, B. Liu, Selective photoelectrochemical oxidation of glycerol to high value-added dihydroxyacetone, Nat. Commun. 10 (2019) 1779, https://doi.org/10.1038/s41467-019-09788-5.

[38] J. Geng, S. Ji, M. Jin, C. Zhang, M. Xu, G. Wang, C. Liang, H. Zhang, Ambient electrosynthesis of urea with nitrate and carbon dioxide over iron-based dual-sites, Angew. Chem. Int. Ed. 62 (2023) e202210958, https://doi.org/10.1002/anie.202210958.

[39] Y. Zhao, Y. Ding, W. Li, C. Liu, Y. Li, Z. Zhao, Y. Shan, F. Li, L. Sun, F. Li, Efficient urea electrosynthesis from carbon dioxide and nitrate via alternating Cu–W bimetallic C–N coupling sites, Nat. Commun. 14 (2023) 4491, https://doi.org/10.1038/s41467-023-40273-2.

[40] M. Rodriguez-Pena, J.A. Barrios Perez, J. Llanos, C. Saez, C.E. Barrera-Diaz, M.A. Rodrigo, Electrochemical generation of ozone using a PEM electrolyzer at acidic pHs, Sep. Purif. Technol. 267 (2021) 118672, https://doi.org/10.1016/j.seppur.2021.118672.

[41] P.A. Christensen, T. Yonar, K. Zakaria, The electrochemical generation of ozone: a review, Ozone Sci. Eng. 35 (2013) 149–167, https://doi.org/10.1080/01919512.2013.761564.

[42] L.M. Da Silva, L.A. De Faria, J.F.C. Boodts, Electrochemical ozone production: influence of the supporting electrolyte on kinetics and current efficiency, Electrochim. Acta 48 (2003) 699–709, https://doi.org/10.1016/S0013-4686(02)00739-9.

[43] S. Stucki, G. Theis, R. Kötz, H. Devantay, H.J. Christen, In situ production of ozone in water using a membrel electrolyzer, J. Electrochem. Soc. 132 (1985) 367, https://doi.org/10.1149/1.2113840.

[44] K. Onda, T. Ohba, H. Kusunoki, S. Takezawa, D. Sunakawa, T. Araki, Improving characteristics of ozone water production with multilayer electrodes and operating conditions in a polymer electrolyte water electrolysis cell, J. Electrochem. Soc. 152 (2005) D177–D183, https://doi.org/10.1149/1.2034551.

[45] P. Tatapudi, J.M. Fenton, Synthesis of ozone in a proton exchange membrane electrochemical reactor, J. Electrochem. Soc. 140 (1993) 3527, https://doi.org/10.1149/1.2221121.

[46] K. Arihara, C. Terashima, A. Fujishima, Electrochemical production of high-concentration ozone-water using freestanding perforated diamond electrodes, J. Electrochem. Soc. 154 (2007) E71–E75, https://doi.org/10.1149/1.2509385.

[47] M.I. Awad, M.M. Saleh, Electrochemical generation of ozone at PbO_2-loaded platinum screens, J. Solid State Electrochem. 14 (2010) 1877–1883, https://doi.org/10.1007/s10008-010-1030-z.

[48] É.C.G. Rufino, M.H.P. Santana, L.A. De Faria, L.M. Da Silva, Influence of lead dioxide electrodes morphology on kinetics and current efficiency of oxygen-ozone evolution reactions, Chem. Pap. 64 (2010) 749–757, https://doi.org/10.2478/s11696-010-0062-2.

[49] Á. Moratalla, S.E. Correia, E. Lacasa, P. Murillo, P. Cañizares, M.A. Rodrigo, C. Sáez, Facing the treatment of polymedicated effluents using gaseous ozone electrochemically generated, J. Water Process 55 (2023) 104153, https://doi.org/10.1016/j.jwpe.2023.104153.

[50] K. Kitsuka, K. Kaneda, M. Ikematsu, M. Iseki, K. Mushiake, T. Ohsaka, Ex situ and in situ characterization studies of spin-coated TiO_2 film electrodes for the electrochemical ozone production process, Electrochim. Acta 55 (2009) 31–36, https://doi.org/10.1016/j.electacta.2009.07.059.

[51] Y.-H. Wang, S. Cheng, K.-Y. Chan, Synthesis of ozone from air via a polymer-electrolyte-membrane cell with a doped tin oxide anode, Green Chem. 8 (2006) 568–572, https://doi.org/10.1039/B516927E.

[52] L.M. Da Silva, D.V. Franco, L.G. Sousa, I.C. Goncalves, Characterization of an electrochemical reactor for the ozone production in electrolyte-free water, J. Appl. Electrochem. 40 (2010) 855–864, https://doi.org/10.1007/s10800-009-0069-y.

[53] K. Zakaria, P.A. Christensen, The use of Ni/Sb–SnO_2-based membrane electrode assembly for electrochemical generation of ozone and the decolourisation of reactive blue 50 dye solutions, Electrochim. Acta 135 (2014) 11–18, https://doi.org/10.1016/j.electacta.2014.05.013.

[54] M. Rodríguez-Peña, J.A. Barrios Pérez, J. Llanos, C. Saez, C.E. Barrera-Díaz, M.A. Rodrigo, Toward real applicability of electro-ozonizers: Paying attention to the gas phase using actual commercial PEM electrolyzers technology, Chemosphere 289 (2022) 133141, https://doi.org/10.1016/j.chemosphere.2021.133141.

[55] M. Rodríguez-Peña, J.A. Barrios Pérez, J. Lobato, C. Saez, C.E. Barrera-Díaz, M.A. Rodrigo, Influence of pressure and cell design on the production of ozone and organic degradation, Sep. Purif. Technol. 297 (2022) 121529, https://doi.org/10.1016/j.seppur.2022.121529.

[56] L.M. Da Silva, L.A. De Faria, J.F.C. Boodts, Green processes for environmental application. Electrochemical ozone production, Pure Appl. Chem. 73 (2001) 1871–1884, https://doi.org/10.1351/pac200173121871.

[57] Q. Zhang, Y. Cao, Y. Yan, B. Yuan, H. Zheng, Y. Gu, X. Zhong, J. Wang, Synergetic effect of pyrrolic-N and doped boron in mesoporous carbon for electrocatalytic ozone production, J. Mater. Chem. A 8 (2020) 2336–2342, https://doi.org/10.1039/c9ta12866b.

[58] G.L. Putnam, R.W. Moulton, W.W. Fillmore, L.H. Clark, Electrolytic ozone, J. Electrochem. Soc. 93 (1948) 211, https://doi.org/10.1149/1.2773807.

[59] Y. Yan, Y. Gao, H. Zheng, B. Yuan, Q. Zhang, Y. Gu, G. Zhuang, Z. Wei, Z. Yao, X. Zhong, X. Li, J. Wang, Simultaneous electrochemical ozone production and hydrogen evolution by using tantalum-based nanorods electrocatalysts, Appl. Catal. B Environ. 266 (2020) 118632, https://doi.org/10.1016/j.apcatb.2020.118632.

[60] Y. Du, L. Hao, W. Zixuan, W. Xi, M. Guirong, W. Xu, Facile synthesis of β-PbO_2 nanoparticles range from 10–30 nm and their application for ozone generation, J. Electrochem. Soc. 168 (2021) 123504, https://doi.org/10.1149/1945-7111/ac40c6.

[61] X. Wang, D. Wu, H. Ge, L. Wang, X. Wu, Shape-controlled synthesis of lead dioxide nanoparticles for enhanced electrocatalysis of electrochemical ozone production, J. Environ. Chem. Eng. 11 (2023) 110248, https://doi.org/10.1016/j.jece.2023.110248.

[62] X. Wang, D. Wu, X. Wu, A long-term-stable continuous flow electrochemical ozone generator with high current efficiency, Sustain. Energy Fuels 7 (2023) 2680–2689, https://doi.org/10.1039/d3se00258f.

[63] F. Okada, S. Tanaka, S. Tanaka, K. Naya, Electrochemical production of 70 wt ppm ozone water, Electrochim. Acta 153 (2015) 210–216, https://doi.org/10.1016/j.electacta.2014.12.010.

[64] M. Rodríguez-Peña, J.A. Barrios Pérez, J. Llanos, C. Saez, C.E. Barrera-Díaz, M.A. Rodrigo, Electrochemical generation of ozone using a PEM electrolyzer at acidic pHs, Sep. Purif. Technol. 267 (2021) 118672, https://doi.org/10.1016/j.seppur.2021.118672.

[65] C.M. Lees, J.L. Lansing, S.L. Morelly, S.E. Lee, M.H. Tang, Ni- and Sb-doped SnO_2 electrocatalysts with high current efficiency for ozone production via electrodeposited nanostructures, J. Electrochem. Soc. 165 (2018) E833–E840, https://doi.org/10.1149/2.0051816jes.

[66] A.M. Mohammad, K. Kitsuka, A.M. Abdullah, M.I. Awad, T. Okajima, K. Kaneda, M. Ikematsu, T. Ohsaka, Development of spin-coated Si/TiOx/Pt/TiOx electrodes for the electrochemical ozone production, Appl. Surf. Sci. 255 (2009) 8458–8463, https://doi.org/10.1016/j.apsusc.2009.06.001.

[67] A. Kraft, M. Stadelmann, M. Wunsche, M. Blaschke, Electrochemical ozone production using diamond anodes and a solid polymer electrolyte, Electrochem. Commun. 8 (2006) 883–886, https://doi.org/10.1016/j.elecom.2006.02.013.

[68] A. Li, S. Kong, C. Guo, H. Ooka, K. Adachi, D. Hashizume, Q. Jiang, H. Han, J. Xiao, R. Nakamura, Enhancing the stability of cobalt spinel oxide towards sustainable oxygen evolution in acid, Nat. Catal. 5 (2022) 109–118, https://doi.org/10.1038/s41929-021-00732-9.

[69] X. Li, D. Pletcher, F.C. Walsh, Electrodeposited lead dioxide coatings, Chem. Soc. Rev. 40 (2011) 3879–3894, https://doi.org/10.1039/C0CS00213E.

[70] X. Wang, D. Wu, L. Wang, X. Wu, Fabrication of novel 3D star-like PbO_2 nanospheres for enhanced electrochemical ozone production, J. Electrochem. Soc. 169 (2022) 106503, https://doi.org/10.1149/1945-7111/ac9435.

[71] J. Wang, X. Li, L. Guo, X. Luo, Effect of surface morphology of lead dioxide particles on their ozone generating performance, Appl. Surf. Sci. 254 (2008) 6666–6670, https://doi.org/10.1016/j.apsusc.2008.04.052.

[72] H. Shi, G. Feng, T. Sun, X. Wang, L. Ding, Z. Wang, H. Jin, Q. Chen, S. Wang, X. Zhong, Y. Zhu, J. Wang, Convex polyhedral nanocrystals with high-index and low-index microfacets for electrochemical co-production of ozone and hydrogen peroxide, Chem Catal. 3 (2023) 100728, https://doi.org/10.1016/j.checat.2023.100728.

[73] J. Wang, X. Jing, Study on the effect of the lead dioxide particles on the anodic electrode performance for ozone generation, Electrochemistry 74 (2006) 539–543, https://doi.org/10.5796/electrochemistry.74.539.

[74] H. Shi, X. Wang, X. Peng, M. Xue, Y. Xue, F. Gao, X. Zhong, J. Wang, Regulation of the microenvironment of Pb_2O_3@Bi_2O_3-tube by structural reconstruction for boosting the electrochemical ozone production performance, J. Mater. Chem. A 12 (2024) 10852–10862, https://doi.org/10.1039/D4TA00719K.

[75] S. Chen, F. Jiang, X. Xie, Y. Zhou, X. Hu, Synthesis and application of lead dioxide nanowires for a PEM ozone generator, Electrochim. Acta 192 (2016) 357–362, https://doi.org/10.1016/j.electacta.2016.01.202.

[76] Q. Yu, X. Hu, Phase/size-controlled synthesis of nanostructured PbO_2 microspheres for efficient electrochemical ozone generation, ChemElectroChem 9 (2022) 301–311, https://doi.org/10.1002/celc.202200919.

[77] H. Shi, G. Feng, S. Li, J. Liu, X. Yang, Y. Li, Y. Lu, X. Zhong, S. Wang, W. Jianguo, Weak Pb–O of confined [Pb–O_4] in pyramidal sillenite-type $Bi_{12}PbO_{20}$ for enhanced electrochemical ozone production, J. Mater. Chem. A 10 (2022) 5430–5441, https://doi.org/10.1039/D1TA10701A.

[78] W. Jiang, S. Wang, J. Liu, H. Zheng, Y. Gu, W. Li, H. Shi, S. Li, X. Zhong, J. Wang, Lattice oxygen of PbO_2 induces crystal facet dependent electrochemical ozone production, J. Mater. Chem. A 9 (2021) 9010–9017, https://doi.org/10.1039/d0ta12277g.

[79] D. Yao, L. Gu, B. Zuo, S. Weng, S. Deng, W. Hao, A strategy for preparing high-efficiency and economical catalytic electrodes toward overall water splitting, Nanoscale 13 (2021) 10624–10648, https://doi.org/10.1039/D1NR02307A.

[80] S.G. Peera, R.S. Menon, S.K. Das, A. Alfantazi, K. Karuppasamy, C. Liu, A.K. Sahu, Oxygen reduction electrochemistry at F doped carbons: a review on the effect of highly polarized C-F bonding in catalysis and stability of fuel cell catalysts, Coord. Chem. Rev. 500 (2024) 215491, https://doi.org/10.1016/j.ccr.2023.215491.

[81] Q. Yu, Z. Jiang, J. Yin, S. Chen, X. Hu, Unraveling the role of F in electrochemical ozone generation on the F-doped PbO_2 electrode, J. Phys. Chem. C 126 (2022) 19397–19408, https://doi.org/10.1021/acs.jpcc.2c05174.

[82] J. Liu, C. Qiu, Z. Xu, M. Xue, J. Cai, H. Shi, L. Ding, X. Li, X. Zhong, J. Wang, Tailoring hydrophobic-aerophilic microenvironment for robust electrochemical ozone production, Chem. Eng. J. 468 (2023) 143504, https://doi.org/10.1016/j.cej.2023.143504.

[83] J. Liu, S. Wang, Z. Yang, C. Dai, G. Feng, B. Wu, W. Li, L. Shu, K. Elouarzaki, X. Hu, X. Li, H. Wang, Z. Wang, X. Zhong, Z.J. Xu, J. Wang, Phase shuttling-enhanced electrochemical ozone production, EES Catal 1 (2023) 301–311, https://doi.org/10.1039/D3EY00015J.

[84] F. Liu, S. Jiang, S. You, Y. Liu, Recent advances in electrochemical decontamination of perfluorinated compounds from water: a review, Front. Environ. Sci. Eng. 17 (2022) 18, https://doi.org/10.1007/s11783-023-1618-z.

[85] J. Liu, S. Wang, J. Cai, L. Wu, Y. Liu, J. He, Z. Xu, X. Peng, X. Zhong, L. An, J. Wang, Synergistic promotion by highly active square-shaped lead oxide and visualized electrolyzer for enhanced electrochemical ozone production, Chin. J. Catal. 57 (2024) 80–95, https://doi.org/10.1016/S1872-2067(23)64614-5.

[86] C. Zhang, Y. Xu, P. Lu, X. Zhang, F. Xu, J. Shi, Capillary effect-enabled water electrolysis for enhanced electrochemical ozone production by using bulk porous electrode, J. Am. Chem. Soc. 139 (2017) 16620–16629, https://doi.org/10.1021/jacs.7b07705.

[87] P.C. Foller, C.W. Tobias, The anodic evolution of ozone, J. Electrochem. Soc. 129 (1982) 506, https://doi.org/10.1149/1.2123890.

[88] B. Yuan, Z. Yao, C. Qiu, H. Zheng, Y. Yan, Q. Zhang, X. Sun, Y. Gu, X. Zhong, J. Wang, Synergistic effect of size-dependent PtZn nanoparticles and zinc single-atom sites for electrochemical ozone production in neutral media, J. Energy Chem. 51 (2020) 312–322, https://doi.org/10.1016/j.jechem.2020.03.066.

[89] Y. Gu, S. Wang, H. Shi, J. Yang, S. Li, H. Zheng, W. Jiang, J. Liu, X. Zhong, J. Wang, Atomic Pt embedded in BNC nanotubes for enhanced electrochemical ozone production via an oxygen intermediate-rich local environment, ACS Catal. 11 (2021) 5438–5451, https://doi.org/10.1021/acscatal.1c00413.

[90] M. Li, C. Qiu, T. Sun, X. Wang, L. Xia, X. Yang, W. Zhao, H. Shi, L. Ding, X. Zhong, Y. Zhu, J. Wang, Frustrating surface segregation by nanoconfinement: boosting electrochemical ozone production over a $B_{13}C_2$-encapsulated PtNi alloy electrocatalyst, Ind. Eng. Chem. Res. 62 (2023) 7889–7900, https://doi.org/10.1021/acs.iecr.3c00389.

[91] S.-A. Cheng, K.-Y. Chan, Electrolytic generation of ozone on an antimony-doped tin dioxide coated electrode, Electrochem. Solid State Lett. 7 (2004) D4, https://doi.org/10.1149/1.1645753.

[92] Y.-H. Wang, S. Cheng, K.-Y. Chan, X.Y. Li, Electrolytic generation of ozone on antimony- and nickel-doped tin oxide electrode, J. Electrochem. Soc. 152 (2005) D197–D200, https://doi.org/10.1149/1.2041007.

[93] P.A. Christensen, W.F. Lin, H. Christensen, A. Imkum, J.M. Jin, G. Li, C.M. Dyson, Room temperature, electrochemical generation of ozone with 50% current efficiency in 0.5m sulfuric acid at cell voltages < 3V, Ozone Sci. Eng. 31 (2009) 287–293, https://doi.org/10.1080/01919510903039309.

[94] X. Wang, J. Li, L. Ding, H. Shi, J. Liu, X. Yang, M. Li, X. Zhong, Z. Yao, J. Wang, Tailoring crystal facet microenvironments for simultaneous electrochemical ozone and hydrogen peroxide production, AlChE J. 69 (2023) e18152, https://doi.org/10.1002/aic.18152.

[95] L. Ding, W. Li, M. Xue, X. Peng, H. Shi, J. Liu, X. Wang, C. Jiang, Y. Xue, S. Wang, X. Zhong, J. Wang, Simultaneous ozone and hydrogen peroxide electrosynthesis via defect modulation in Ni, Sb-doped SnO_2 electrocatalysts, AlChE J. 70 (2024) e18314, https://doi.org/10.1002/aic.18314.

[96] R.N. Mariammal, K. Ramachandran, B. Renganathan, D. Sastikumar, On the enhancement of ethanol sensing by CuO modified SnO_2 nanoparticles using fiber-optic sensor, Sens. Actuators, B 169 (2012) 199–207, https://doi.org/10.1016/j.snb.2012.04.067.

[97] A. Benvidi, M. Karimi, S.M. Bidoki, M.A.K. Zarchi, S. Dalirnasab, M.D. Tezerjani, A. Behjat, Fabrication of several SnO_2-based anodes for electrochemical ozone generation: comparison, characterization and application, Res. Chem. Intermed. 47 (2021) 4803–4824, https://doi.org/10.1007/s11164-021-04551-2.

[98] J.L. Lansing, L. Zhao, T. Siboonruang, N.H. Attanayake, A.B. Leo, P. Fatouros, S.M. Park, K.R. Graham, J.A. Keith, M. Tang, Gd-Ni-Sb-SnO_2 electrocatalysts for active and selective ozone production, AlChE J 67 (2021) e17486, https://doi.org/10.1002/aic.17486.

[99] M. Xue, J. Zhao, X. Yu, L. Ding, X. Wang, J. Liu, H. Shi, Y. Xue, Z. Yao, X. Zhong, J. Wang, Facilitating electrochemical ozone production and chlorine evolution reaction by synergistic effect of multicomponent metal oxides, Adv. Funct. Mater. 34 (2023) 2308567, https://doi.org/10.1002/adfm.202308567.

[100] B. Jin, S. Cheng, Y. Sun, P. Xie, L. Li, High selectivity toward electrochemical ozone production of Sb-SnO_2 with Cu and Ni Co-doped, Adv. Funct. Mater. 34 (2024) 2314144, https://doi.org/10.1002/adfm.202314144.

[101] G.F. Wood, I.M. Terrero Rodríguez, J.J. Tully, S. Chaudhuri, J.V. Macpherson, Electrochemical ozone generation using compacted high pressure high temperature synthesized boron doped diamond Microparticle electrodes, J. Electrochem. Soc. 168 (2021) 126514, https://doi.org/10.1149/1945-7111/ac3ff4.

[102] X. Yang, W. Li, S. Wang, H. Shi, X. Wang, M. Li, L. Ding, X. Zhong, J. Wang, Hybrid sp^3/sp^2 two-dimensional nanodiamonds for electrochemical ozone production, ACS EST Eng. 3 (2023) 894–905, https://doi.org/10.1021/acsestengg.2c00449.

[103] F. Liu, Z. Deng, D. Miao, W. Chen, Y. Wang, K. Zhou, L. Ma, Q. Wei, A highly stable microporous boron-doped diamond electrode etched by oxygen plasma for enhanced electrochemical ozone generation, J. Environ. Chem. Eng. 9 (2021) 106369, https://doi.org/10.1016/j.jece.2021.106369.

[104] Y. Nishiki, N. Kitaori, K. Nakamuro, Performances of small-sized generator of ozone-dissolved water using boron-doped diamond electrodes, Ozone Sci. Eng. 33 (2011) 114–120, https://doi.org/10.1080/01919512.2011.549411.

[105] M. Lu, X. Liu, C. Jing, X. Wang, L. Ding, F. Gao, L. Ren, S. Dai, X. Zhong, J. Wang, Efficient electrochemical ozone and hydrogen peroxide production by synergistic effect of atomically dispersed Pt, boron and nitrogen doped 2D diamonds, Adv. Funct. Mater. (2024) 2412170, https://doi.org/10.1002/adfm.202412170.

[106] P.V. Nidheesh, G. Divyapriya, N. Oturan, C. Trellu, M.A. Oturan, Environmental applications of boron-doped diamond electrodes: 1. Applications in water and wastewater treatment, ChemElectroChem 6 (2019) 2124–2142, https://doi.org/10.1002/celc.201801876.

[107] D. Clematis, M. Panizza, Application of boron-doped diamond electrodes for electrochemical oxidation of real wastewaters, Curr. Opin. Electrochem. 30 (2021) 100844, https://doi.org/10.1016/j.coelec.2021.100844.

[108] X. Peng, Z. Bao, S. Zhang, Y. Li, L. Ding, H. Shi, J. Liu, X. Zhong, X. Li, J. Wang, Modulation of Lewis and Brønsted acid centers with oxygen vacancies for Nb_2O_5 electrocatalysts: towards highly efficient simultaneously electrochemical ozone and hydrogen peroxide production, Chem. Eng. Sci. 271 (2023) 118573, https://doi.org/10.1016/j.ces.2023.118573.